Eidgenössische Technische Hochschule Zürich
Swiss Federal Institute of Technology Zurich

RF wiring design for a multi-channel cryogenic cQAD experiment

Semester Project FS 2022

Francesco Maria Ruscio
fruscio@student.ethz.ch

MSc Quantum Engineering

Laboratory for Solid State Physics
Departement of Physics, D-PHYS
ETH Zürich

Supervisors:
Marius Bild
Prof. Dr. Yiwen Chu

July 8, 2022

I am thankful to my supervisor, Marius, since he helped me a lot during the project and was always available to discuss my ideas and clarify my doubts.

I would also like to thank Matteo, Yu and Yiwen for the fruitful discussions and explanations.

I am also very grateful to all Gandalf Team since everyone helped me with the cables' preparation and testing.

Finally, thanks to Michael for all the free biscuits and the fun in F10 and to all HyQu group for all the pleasant activities we have done together in the last months.

Abstract

This project aimed to reorganize the baseplate setup of the diluition refrigerator in F11, adding new microwave components.
In order to achieve the goal of the project, different designs for the allocations of the baseplate components and the cabling setup have been modeled on Inventor. It has been finally chosen the more compact solution that leads to a more handy cabling solution.
After it, the newly designed parts have been prepared by the workshop and the new cables have been prepared by us in F14, following specific constraints on them.
In the end, all the design has been mounted inside the refrigerator.

Contents

Chapter 1

Introduction

In the last century all the fields related to people's lives have experienced a rapid technological improvement. The birth of electronics and information technology science has the right to be considered as one of the most important technological innovations we, as humanity, have faced. Thanks to Moore's law, these two disciplines have opened to us new unexpected doors, from the possibility to share in real time our experiences in social networks to the ability to efficiently simulate turbulent flows around the wing of an aeroplane. Nevertheless, the more knowledge we acquire about the world using computers, the more eager we are to discover new phenomena, usually requiring more computational power. Moreover there are some well known problems, for example the simulation of quantum systems, that we cannot simulate properly with classical computers [1].

Quantum technologies, and in particular *quantum computers*, aim to solve these two problems exploiting two cornerstones of quantum mechanics, the superposition principle and the entanglement principle. Addressing directly the previous discussion, it has been demonstrated that quantum algorithms can easily tackle problems that are computationally hard to solve with classical algorithms, for example the integer factorization of a number [2]. In addition to this, since quantum computers are by construction quantum systems, they can be used to efficiently simulate other quantum systems [3], for instance they can be exploited to study new molecules to engineer medicines.
Even if quantum computers are believed to be able to enhance us with currently inaccessible solutions to several questions and problems, we still do not possess a universal quantum computer. For this reason, there is a genuine competition among a lot of research groups around the world to build a *quantum processor*; at the state of the art, the two most promising physical platforms to create a quantum computer are *superconducting circuits* and trapped ions. It is possible to classify them as belonging to the NISQ era [4], which comprises technologies capable to partly surpass the abilities of classical computers, but still characterized by noisy quantum gates.
In the meantime, a question naturally arises: can we use quantum properties of the nature not only to build new computers but to reshape the entire information technology science? Trying to answer to this question, newly born researches focus on **quantum memories**, quantum communication and quantum networks.

1.1. Circuit Quantum Acousto-dynamics

Circuit Quantum Acousto-dynamics (cQAD) is the field that describes artificial atoms from cQED, i.e. *circuit quantum electrodynamics*, coupled to *quantum acoustic* systems, i.e. mechanical oscillators. It is strongly related to electromechanics since the coupling between the different systems can be described in the framework of this theory.
CQED transfers the knowledge acquired in quantum optics to superconducting circuits; an LC circuit is equivalent to an optical resonator and a non-linear LC circuit, e.g. obtained by substituting the inductor with a josephson junction, represents an artificial atom. A superconducting circuit made up of a capacitor and a josephson junction is the basic block of a quantum information platform in this physical system; this is because it has a non-linear energy spectrum, equivalent to the spectrum of a non-linear optical resonator, and can be used as a *qubit* [5]. There exist other types of superconducting qubits [6], since to realize a qubit it is just needed a superconducting platform characterized by a non-linearity in the energy spectrum.
Quantum acoustic studies the mechanical modes of solid-state systems in the quantum regime[7]. In more detail, phonon formalism is used to describe the quantum properties of the acoustic modes in massive objects, e.g. phononic crystals. These systems can generally behave as multimode mechanical oscillators.

CQAD studies platforms composed of superconducting circuits coupled to mechanical resonators in the quantum regime, resulting in *quantum hybrid systems* [8]. One example for such a systems is shown in Figure 1.1.

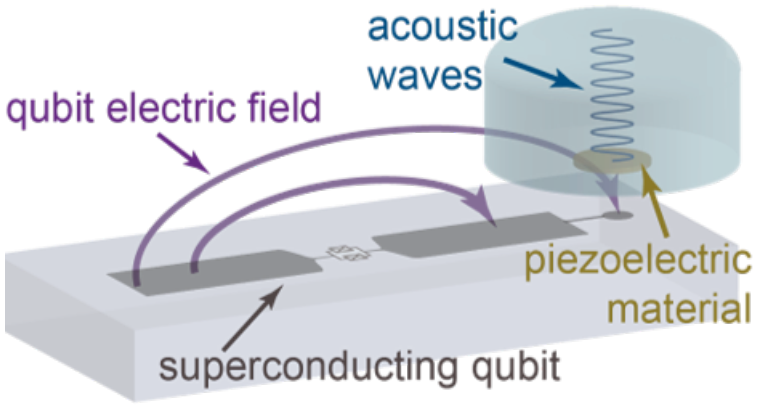

Figure 1.1.: Superconducting flux tunable qubit with an antenna connected to one of the capacitive pads of the qubit, used to improve electromechanical coupling. The antenna is aligned with a piezoelectric transducer, connected to the substrate of a high overtone bulk acoustic wave resonator (HBAR).

An HBAR is a bulk acoustic wave (BAW) resonator that confines high overtone longitudinal bulk waves, characterized by frequencies in the GHz regime, in the direction of propagation. The qubit is coupled to the HBAR, forming a device called $\hbar BAR$. The

coupling is achieved exploiting the piezoelectric transducer, since the qubit's electric field is converted into mechanical strain in the piezoelectric material; the strain then propagates into the bulk of the HBAR. The coupling is enhanced by the antenna, used to have more overlap between the qubit's electric field and the transducer. In this way it enables a resonant swap of an excitation between the qubit and the phononic states of the HBAR. Among various and interesting experimental results, it has been shown that the qubit can be strongly coupled to the BAW resonator [9], in which it is even possible to generate a multi-phonon Fock state[10].
This device opens the possibility to control at the quantum level macroscopic objects, since the massless photons in cQED have been substituted here by phonons characterized by a finite effective mass.
The ability to coherently swap energy between the qubit and the HBAR in such a cQAD systems can lead, among other possibilities, to the design of *quantum memories*, because, for instance, a quantum processor could process the information exploiting the superconducting circuit and then the qubit states can be stored in the low loss modes of the HBAR, effectively behaving as a memory [11].

1.2. Motivations and Goals

CQAD systems, in order to be operated in the quantum regime, require specific instrumentation, mostly deriving from that needed for cQED experiments. It is extremely important to consider that both the superconducting qubits and the mechanical oscillators are not pure two level systems, but they have an energy spectrum characterized by infinite levels, such that, in principle and in practice, many different states of these systems are occupied.
Considering only the superconducting circuit, it can be considered a qubit since it has an anharmonic energy spectrum and it is possible to achieve the situation in which only two states have a probability of being occupied different from zero. These states are called computational basis states and they usually are the ground state and the first excited state of the system. The energy difference between these states is the transition frequency of the qubit; common values for it are $\nu \approx 5 - 6$ GHz. Following the last description, it is easy to understand that the superconducting circuit will behave as a qubit only if its higher excited states are not thermally occupied. For this reason, since $T = \frac{h\nu}{k_B} \approx 240 - 290$ mK, we need to keep the qubit at very low temperatures using an appropriate commercial dilution refrigerator.

During this project I have worked on one refrigerator of the *Hybrid Quantum Systems Group*. The two main goals of the project are:

1. Reorganization of the different parts of the experimental setup at baseplate of the refrigerator to have the possibility to have four different *complete* sets of radiofrequency (RF) lines for four different experiments. This topic is discussed in chapter 3.

2. Design of the new RF cables at the baseplate of the refrigerator to have a more handy setup for the change of the platoforms for the experiments. The design solution is presented in chapter 4.

The report consists of three main chapters. Chapter 2 describes the type of dilution refrigerator used in the laboratory and the usual microwave setup exploited in the refrigerator for cQAD experiments. Chapter 3 summarizes the first part of my work, focused on the study of a new setup for the baseplate of the refrigerator. Finally, chapter 4 describes the new RF wiring design that will be used at the baseplate of the refrigerator.

Chapter 2

Millikelvin Engineering

As discussed in chapter 1, we need to run our experiments at very low temperatures, usually in the order of $T_{exp} \sim 10$ mK, to observe the quantum properties of our devices. It is also important to note that, since we are using superconducting materials, it would not be possible to have a functioning qubit if the chip to be tested was at room temperature, being above the critical temperature for superconductivity.
In order to achieve sub-Kelvin temperatures, a special type of refrigerator, called **dilution refrigerator**, is used. Moreover, it is not possible to use room temperature electronic components for the microwave's regime, but it is mandatory to use devices engineered to function at the aforementioned temperatures. This chapter provides an introduction to these topics related to the project's subject.

2.1. Dilution refrigerators

Among all the different types of refrigerators, dilution refrigerators (DRs) are the only ones that guarantee continuous cooling to temperatures down to 2 mK. They are widely used in the field of quantum computing for mainly two reasons:

- Have the possibility to exploit a physical systems as a superconducting qubit, avoiding thermal excitations to higher excited states of the system and providing an efficient initialization to the ground state, one of the two computational basis states.
- Suppress thermal noise on the signals used to control and readout the qubits.

There exist several kinds of DRs, engineered to work in very different and specific situations, e.g. they can be designed to function in space as the one used in the Planck satellite [12]. This section contains a brief description of *dry DRs*. Before describing a DR itself, it is convenient to describe the properties of a mixture of ^{3}He and ^{4}He at very low temperature, since it is the physical system exploited by the DR for the cooling mechanism.

2.1.1. ^{3}He - ^{4}He mixture

^{4}He particles are bosons and ^{3}He ones are fermions. As far as the ^{4}He particles are concerned, when cooled below 2.17 K, they will undergo a phase transition to a superfluid [13]. The fermionic ones, since they need to obey Pauli's exclusion principle, do not follow a Bose-Einstein condensation [14]. For this reason, a mixture of the two isotopes at low

temperature is described as an inert superfluid system with a weakly-interacting Fermi-gas in it [15]. A phase diagram of the system is shown in Figure 2.1 .

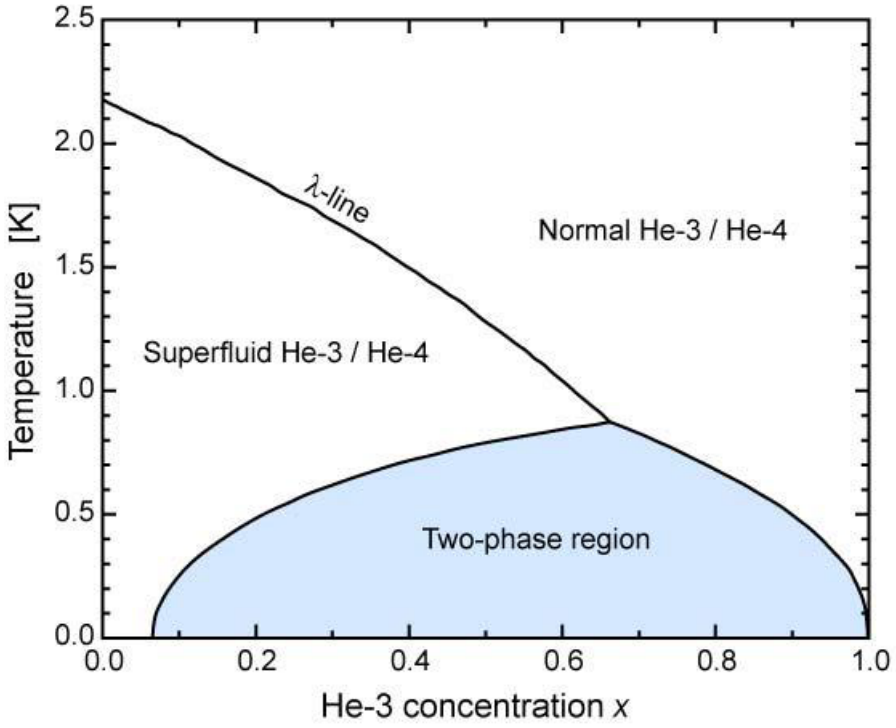

Figure 2.1.: Phase diagram of a ^{3}He - ^{4}He mixture. The figure is taken from [16]

From the phase diagram it is possible to see that the superfluid transition temperature decreases as x_3, the concentration of ^{3}He, increases in the mixture. The blue region is a prohibited region and it is possible to evince from the figure that, if $x_3 > 0.066$ and if $T < 0.87$ K, the mixture is separated into two phases, a dilute one, in which x_3 is low, and a concentrated one. The dilute phase has higher density and enthalpy compared to the concentrated one. Therefore, the concentrated phase floats on top of the dilute phase. Moreover, in order to move ^{3}He atoms from the concentrated phase to the dilute phase, an additional external energy is required [16]. In a DR, this additional energy is taken from the surrounding envinronment, leading to cooling.

2.1.2. Dry dilution refrigerator

A DR exploits the heat of mixing of the two aforementioned isotopes of helium to achieve a cooling to $T \sim 10$ mK. Before running a cooling cycle, a DR needs to be precooled to nearly 4 K. A dry DR, also called *cryogen-free DR*, uses pulse tube coolers for the precooling stage instead of exploiting a liquid helium bath (*wet DR*) [17]. Pulse tube coolers are based on the Stirling engine. The DR in the laboratory looks like the one in

Figure 2.2.

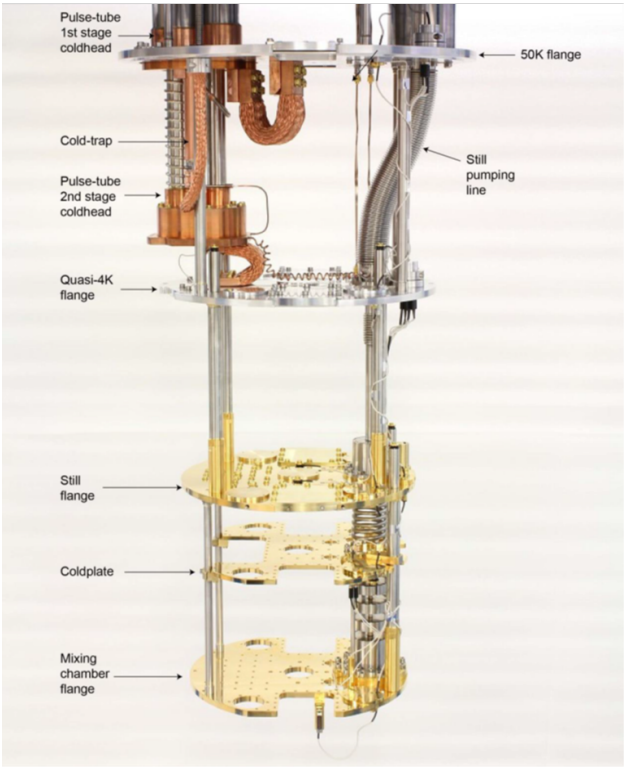

Figure 2.2.: Example of a Bluefors LD-400 dry DR, also used in the laboratory. The shiny gray cylinder on top of the MXC flange is the mixing chamber. The figure is taken from [16]

Referring to Figure 2.2, there are different flanges, also called plates, in a DR and each of them is characterized by a different range of temperatures when the DR is on. Considering only the three coldest plates, i.e. the still flange, the coldplate and the mixing chamber (MXC) flange, typical values for their temperature when the DR is operating are $T_{still} = 900$ mK, $T_{cold} = 100$ mK and $T_{MXC} = 10$ mK [18].

Following the precooling stage, there is a specific procedure that leads the refrigerator to function in the expected condition. The procedure is shortly outlined in the following paragraph, but it is well described in the Bluefors manual for the DR used in the laboratory [16]. First of all, the ^{3}He -^{4}He mixture is condensed by raising the pressure on it and precooling it using heat exchangers. After having created enough condensed mixture to occupy all the *mixing chamber* (MXC) , the heat exchangers and, partly, the *still*, the DR is in the normal operation mode. Its principle of working is shown in Figure 2.3. To obtain the two separated phases of the mixture, helium is pumped out from the Still using the pumping line. This process, thanks to evaporative cooling, leads to a temperature of the mixture below 0.87 K, where it undergoes the described phase transition. Since the

dilute phase is heavier, it will accumulate at the bottom of the MXC and, eventually, the mixture will reach the situation shown in the figure. Continuing pumping out the helium from the Still, considering the vapor pressures of the two isotopes, nearly only the ^{3}He will leave the Still, as can be inferred from Figure 2.3. The ^{3}He is then repumped in through the condensing line, undergoing a precooling mechanism shown as red arrows in the figure. The cooling is obtained since the ^{3}He rich phase is pushed to flow into the dilute phase in the Mixing chamber.

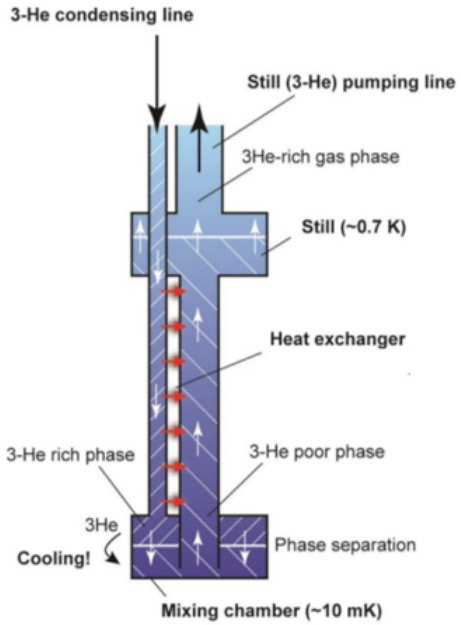

Figure 2.3.: Working principle of a DR. The figure is taken from [16]

2.2. Radiofrequency lines and cryogenic setup

The experimental devices are thermally anchored to the MXC plate (also called baseplate of the DR), such that they are in the right temperature regime for quantum computing applications. Nevertheless, room temperature (RT) electronic is used to generate the driving pulses to control the experiments and, furthermore, the output signal needs to be analysed with electronic components at RT. For this reason, we need to use an experimental setup that is able to transfer the signal from room temperature to sub-Kelvin temperatures and vice versa. To achieve it, RF cables are used to send signals across the setup and proper microwave components, engineered to work at the different temperature stages, are used. In the following pages the setup used in our laboratory is depicted, considering mostly all the necessary parts to properly describe it at the baseplate of the refrigerator. A detailed description of a possible cryogenic setup for quantum computing

applications can be found in [18].

The RF cables used in the setup are coaxial waveguides for microwave signals. They are composed by an inner conductor, a dieletric and an outer conductor. The conductors are made of copper. Since they are used to interact with the cQAD devices, they need to guarantee a high transmission coefficient in the $4 - 8$ GHz frequency range. It is important to notice that the cables concerning my project are not characterized by passive heat load due to heat flow since both extremities of the cables are anchored to the baseplate and there is not a temperature gradient along the cable [18].
On the other hand, as far as microwave components are concerned, since the signal used in the experiment has usually very low intensity, they need to be characterized by low noise such that the noise does not overcome the signal we are interested in. Moreover, each of them needs to be thermally anchored to the MXC plate such that the thermal noise generated does not affect the experiment.

2.2.1. Experimental setup

Each cQAD device we would like to test is placed into 3D a microwave cavity that acts like a readout resonator for our devices. As stated before, we are able to allocate in the DR four different experiments; therefore, we can put four different cavities in the refrigerator. To run our experiment at the required temperature, each cavity should be in thermal contact with the MXC plate. To achieve the right thermalization, two equal brackets, made of OHFC copper, are screwed to the lower part of the baseplate such that they are in thermal contact with it. Two cavities are mounted on each bracket. A magnetic shield around the cavities is used to screen the experiments from the electromagnetic noise in the environment, shown in Figure 2.4.

Each cavity is connected to the control electronics with an input port and an output port. Moreover, we need two more lines for each experiment, as it will be explained later in this chapter. For example, considering the first cavity, the wiring setup and the cryognenic microwave components needed are shown in Figure 2.5.

Each line has a specific name. Apart from the input line ("I", also called drive line) and the output line ("O"), shown also are the pump line ("P") and the diagnostic line ("D"). These four lines together form a set of lines (SL) for a single experiment. Since we can host four experiments at the same time in the DR, there are a total of 16 lines going from room temperature to the MXC plate. During my project I have worked on the part of the lines below the mezzanine (MZ) plate.

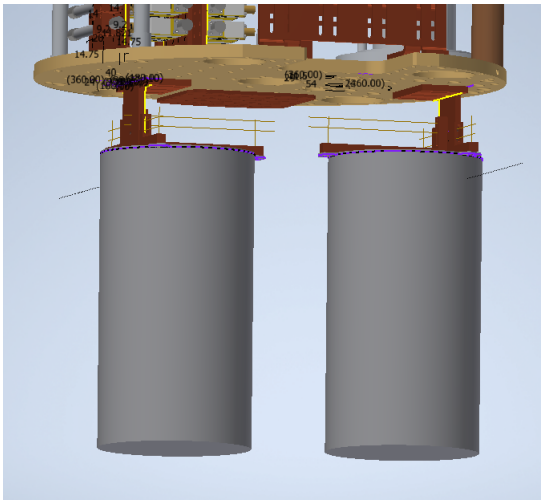

Figure 2.4.: Inventor representation of the brackets holding the cavities with the cylinder-shaped magnetic shields around them. The positions of the brackets are the same locations in the real DR.

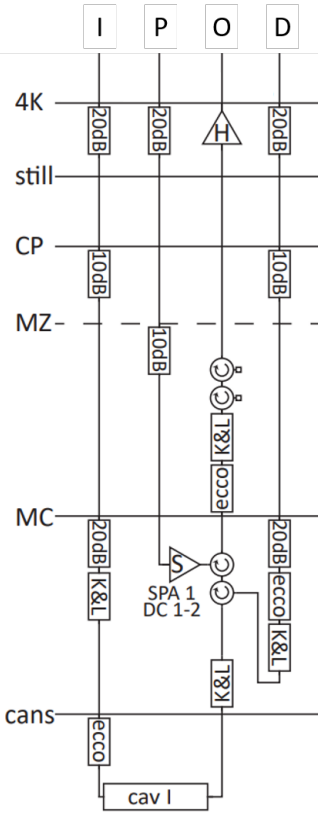

Figure 2.5.: Schematic of the different radiofrequency lines needed to test a $\hbar$BAR device. Each line has a specific name. The different temperature stages of the DR are also shown in the image. "MZ" consists of an OFHC copper cable thermalization plate anchored at the MXC plate.

2.2.2. Lines and components description

In the following section are described the lines shown in Figure 2.5.

Input line

The input line is used to control the cQAD device. Since drive signals are generated at RT, exploiting a microwave generator, an arbitrary waveform generator and an IQ mixer, and considering that we want a very low level of noise on the sample, it is necessary to attenuate the signal at different temperature stages. The number of thermal noise photons generated at a certain temperature stage (T) and at a given frequency (ν), due to blackbody radiation, is given by the Bose-Einstein distribution:

$$n_{BE}(T,\nu) = \frac{1}{e^{\frac{h\nu}{k_B T}} - 1} \tag{2.1}$$

Considering $T_{room} = 300$ K and $\nu = 6$ GHz the noise photons generated at the input of the line are $n_i \approx n_{MB} \approx \frac{k_B T}{h\nu} \approx 1000$, where n_{MB} is the Maxwell-Boltzmann distribution. This noise level is too high to control a cQAD device at the quantum level. To reduce it, three different attenuators are used along the line, each of them thermalized at a particular temperature stage, such that the blackbody radiation emitted by it is low and follows from the temperature of a particular stage. An attenuator that reduces the signal's power by a factor of A effectively behaves as a beam splitter, where the relation between input and output noise photon occupation n_i and n_o, at the temperature T at which the attenuator is thermalized, is given by [19]:

$$n_o(\nu) = \frac{n_i(\nu)}{A} + \frac{A-1}{A} n_{BE}(T,\nu) \tag{2.2}$$

Combining Equation 2.1 and Equation 2.2 it is possible to calculate the thermal noise photon number at the MXC plate, which results to be $n_{MXC} \approx 2 \cdot 10^{-2}$ for our configuration of attenuators, a sufficient value to have coherent control of our device. For this calculation it has not been taken into account the attenuation of the signal along the cables themselves. In addition to the previous consideration, the attenuators are distributed along the line because if we placed a 50 dB attenuator, for example at the baseplate, the heat load due to signal dissipation would exceed the cooling power at the MXC plate, resulting in a temperature increase. Finally, it is not true that adding more attenuation is always useful because the attenuation itself at each temperature stage is limited by the thermal noise floor at that particular stage. This discussion concerning attenuators is also valid for the pump and diagnostic lines.
Along the input line, after the last attenuation stage, are also positioned a K&L filter and an Eccosorb filter. The Eccosorb filter is used to filter out infrared radiation that goes towards the sample. IR radiation needs to be strongly suppressed because, when hitting a superconducting material, it generates Bogoliubov quasiparticles [20], offering a new decay channel to the qubit, reducing the T_1 time [21]. The K&L filter is a low-pass filter

that screens high frequency components of noise, suppressing decoherence mechanisms.

Output line

The output line is used to transfer the signal from the sample back to the RT electronics, where the signal can be analyzed. Along this line, besides the other microwave components, the devices present are:

- *Circulators.* These are three-ports non reciprocal devices. They are built in a way that a signal entering the component in one port can only exit from it from another predefined port. A schematic representation is shown in Figure 2.6.

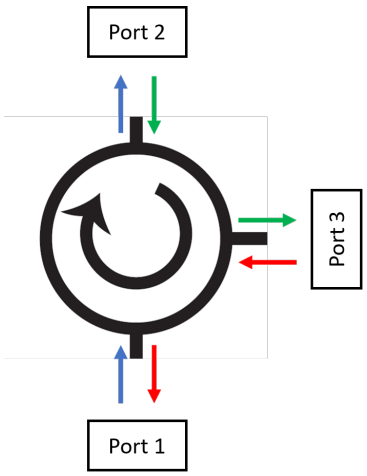

Figure 2.6.: Working principle of a circulator.

  A circulator exploits magnetic fields to circulate the RF signal in one direction. In this way the signal experiences low loss in the black arrow direction, but high loss in the opposite direction. For this reason, a signal entering from one port, e.g. port 1, can only exit from a specific port, e.g. port 2.

- *Isolators.* These are two-ports non reciprocal devices. An isolator behaves like a circulator in which port 3 has been terminated. A signal entering in port 1 will be transmitted to port 2, but a signal entering in port 2 will be absorbed. Summarizing, it is a component that permits the trasmission of signals only in one direction.

Since the output signal from the resonator is very low, and can be estimated to be $P_{out} \approx -130$ dBm, it is necessary to amplify it before reading it out. The presence of a quantum limited amplifier on the readout line is of a crucial importance for a cQAD experiment. To explain this sentence, let's consider an usual amplification chain used in cQED experiments:
From a quantum perspective, each amplifier is characterized by its gain and by the number of noise photons introduced. It is possible to show that the effective gain of the

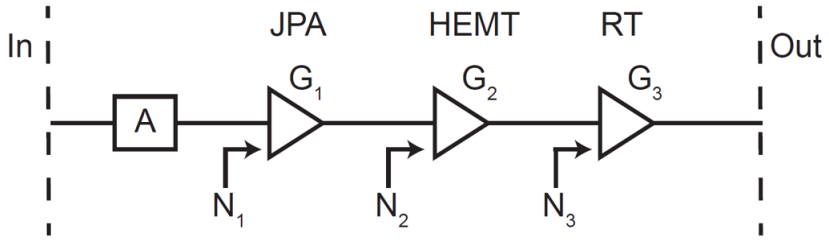

Figure 2.7.: Typical schematic representation of an amplification chain used with superconducting qubit experiments in a readout line. It has three steps of amplification, where the JPA is the quantum limited amplifier. "A" takes into account the attenuation along the cable. Image taken from [19].

chain is given by $G_{eff} = \frac{G_1 G_2 G_3}{A}$ and the total added noise due to all the amplification stages is:

$$N_{out} = (\frac{A-1}{A} + N_1)G_1 G_2 G_3 + N_2 G_2 G_3 + N_3 G_3 \tag{2.3}$$

The noise due to the attenuator takes into account the fact that the noise photons at very low temperature are negligible, but at least one photon is added by the vacuum fluctuations. From Equation 2.3, the effective noise introduced by the amplification chain is given by:

$$N_{eff} = A - 1 + N_1 A + N_2 \frac{A}{G_1} + N_3 \frac{A}{G_1 G_2} \tag{2.4}$$

If the gain G_1 of the quantum limited amplifier is high enough, the effective noise of the chain can be approximated as:

$$N_{eff} \approx A - 1 + N_1 A \tag{2.5}$$

In conclusion, using an amplifier with large gain in the first stage permits an amplification of the signal where the added noise is only due to the first amplifier. If the amplifier is quantum limited, since the added noise will be such that $N_1 \ll 1$, the level of the noise will remain very low. In this way, ideally, the amplification chain, excluding the attenuation part, does not add noise to the readout resonator output.

Describing the line from the cavity to higher temperature stages, the signal is routed, using two circulators, to an SPA and then back on the output line. The SPA, *Snail Parametric Amplifier*, is the quantum limited amplifier used in the laboratory. The signal will then be transmitted along the cable reaching an HEMT (*High-electron-mobility-transistor*) amplifier at 4 K. After it, the signal is routed to the RT electronics. The two isolators between the MXC plate and the MZ stage are used to block possible noise components travelling from the RT devices towards the sample, such that the sample is not wrongly driven. In addition to those, since they are engineered to work mostly in the frequency regime of the cQAD device and the readout resonator, Eccosorb filter and

K&L filters are also positioned along the line to filter out other frequency components of the noise.

Pump line and SPA

As aforementioned, an SPA has noise performance close to the quantum limit [22]. In the following description I will only focus on the SPAs used in the *HyQU Group*. An SPA, as used in our laboratory, is a phase preserving amplifier, i.e. the quadratures of the incoming signal are amplified in the same way. It behaves like a non-linear crystal used to obtain a non-degenerate three-wave mixing. It has to be pumped by a strong signal at frequency ν_{pump} and it amplifies a signal at ν_{signal}, such that $2\nu_{signal} \sim \nu_{pump}$. In order to do so, a photon from the pump is converted in a photon of the signal and, in order to preserve the energy, it is also generated a photon in another mode, called the idler mode, such that:

$$\nu_{pump} = \nu_{signal} + \nu_{idler}$$

This is a down-conversion process characterized by the amplification of the signal and by the generation of some noise photons, detuned from the signal frequency, in the idler mode. A more detailed description of SPAs can be found in [23]
The pump line is used to send the pump signal to the SPA.

Diagnostic line

This line is used to probe the SPA. Let's consider a signal sent on this line; once arrived at the first circulator, it will be routed to the cavity. If the signal is detuned from the resonance frequency of the cavity, it will be reflected by the cavity itself, and it will bounce back towards the circulator, now following the path of a signal on the readout line. Since the signal does not interact with the cQAD device but only with the SPA, the readout signal obtained at RT can be used to characterize the SPA.

2.2.3. State of the art of the DR

Before my semester project, the DR in the laboratory could already host four different cavities at the baseplate. In the last cooldown before the application of my design, the refrigerator hosted the four sets of lines shown in Figure 2.8. It is possible to see that two experiments are executed without using an SPA, reducing the signal to noise ratio of the readout signal compared to the lines with an SPA. Moreover, a part of the setup was not well organized at the MXC plate, resulting in the fact that a lot of RF cables were obstructions during the replacement of the cavities. Due to this, cables sometimes had to be moved to properly work on the cavities, leading to increased probabilities of damaging and breaking cables. Finally, it was not immediate to recognize the line number of a cable from its position.
During the last semester I have worked on these problems and the result of my work is shown in the next two chapters.

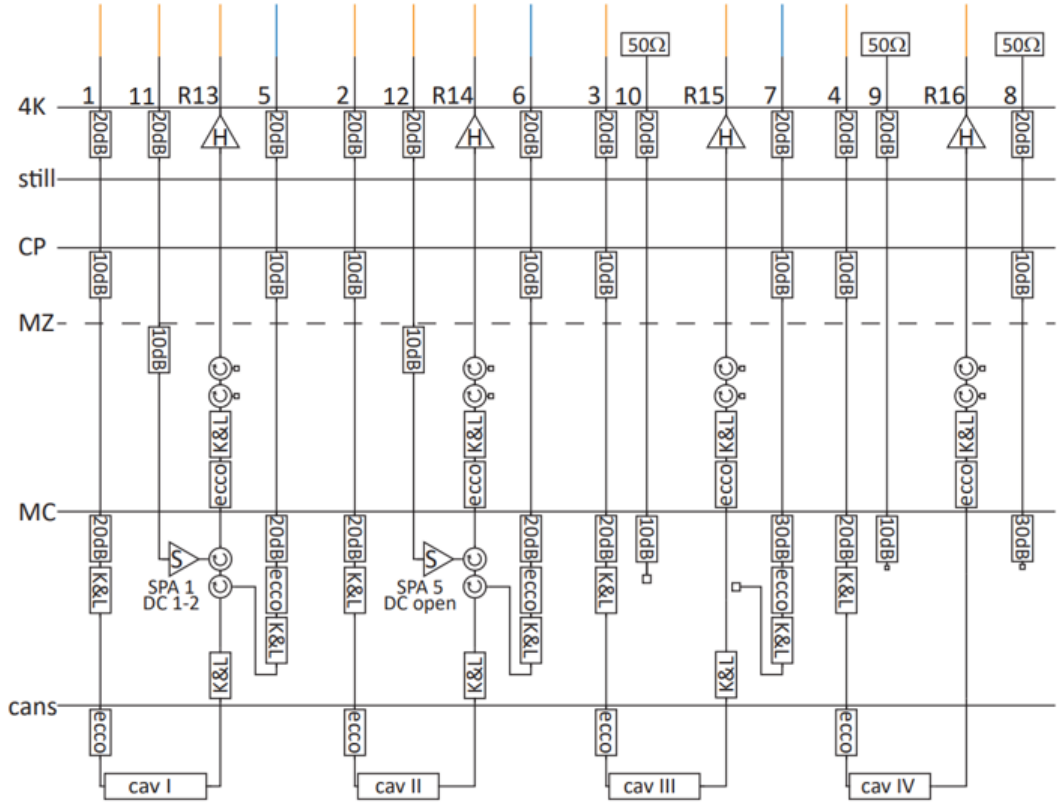

Figure 2.8.: Schematic of the full microwave setup inside the DR during the 25/04/2022 cooldown.

Chapter 3

New Baseplate Setup

In this chapter is presented the new microwave components' setup for the baseplate of the DR; in particular, it is shown the setup that will be mounted in the refrigerator. Other examples of possible design solutions are summarized in Appendix A, but it is possible to find many more prototypes in my personal folder in the *HyQu group drive*.
A reorganization of the microwave components was needed for mainly three reasons:

- Obtaining four *complete* sets of lines in the refrigerator, including the two missing SPAs.
- Have a compact grouping of the devices on the different lines.
- Ensuring a smarter arrangement of the baseplate RF cables, reducing problems deriving from their spatial positions.

As a first step to achieve these goals, the position of the different parts, e.g. the samples' can, in the refrigerator has been measured and modeled in Inventor, a CAD software. I have considered as fixed the arrangement of the cables and electronic components above the mezzanine stage. Moreover I have not changed the microwave components's configuration on the input and diagnostic lines; also the location of the samples' cans is unchanged. Therefore I have studied a new allocation of the SPAs and the different devices on the output line.

3.1. Microwave components' allocation

Considering the output line in Figure 2.5 from the cavity to the 4K stage, to have a better design solution, the cryogenic electronic components have been divided into three groups:

1. First group: K&L filter just after the cavity and first circulator on the line.
2. Second group: second circulator on the line and SPA.
3. Third group: devices between the MXC plate and the MZ stage in the figure. They already had a compact and space saving arrangement, shown in section A.1.

In order to obtain a more realistic and precise estimation of the distance between the I/O ports of the different components, I have also modeled the different connectors, represented in the next images by cylinders of different colours and lengths.

3.1.1. First group arrangement

Each output line needs a K&L filter and a circulator after the cavity, connected together as shown in Figure 3.1a. The cryogenic circulator is linked to the filter (long gray cylinder) thanks to an elbow SMA connector (golden connector). The shiny gray short cylinders are connectors.

To group them for the four output lines, a new OFHC copper bracket has been designed, shown in figure Figure 3.1b, where it is possible to screw the circulators. OFHC stands for *Oxygen-free high thermal conductivity copper*. The bracket's drawing for the workshop can be found in section A.3, together with the drawings of the other parts designed, later described in this chapter. The bracket has a 3 mm width and the bend between the two flat parts is characterized by a bending radius of 3.18 mm. As a general rule, if a sheet of copper has a 3 mm width, each bend should be characterized by a bending radius such that $R_{bending} > 3$ mm. This last consideration ensures that the metallic sheet is not stressed too much. On the vertical part of the bracket in Figure 3.1b are designed eight holes, such that each circulator can be screwed with four screws, achieving the best contact possible between the circulator and the bracket. Moreover, in the final setup, the circulators should be screwed such that they are as low as possible, as explained by Figure 3.1c. The horizontal part of the bracket is then attached to the lower part of the MXC plate and, due to the length of the hole, five different screws can be used to guarantee a good contact between the two; from a practical point of view only two or three screws are sufficient.
A cable, used to link the first circulator of a line to the second of the same line, is connected to the input port of the circulator ("Port 1" in Figure 2.6). The diagnostic line is connected to the output port of the circulator ("Port 2" in Figure 2.6) and the output line, arriving from the sample, is connected to the K&L filter.

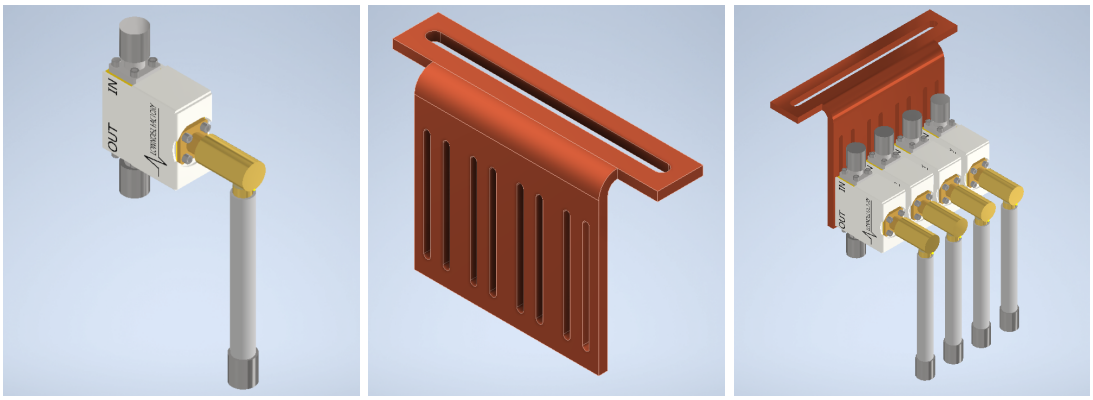

a First group's building block. **b** Circulator's bracket. **c** First group final design.

Figure 3.1.: Figures representing the arrangement of the devices composing the first group.

3.1.2. Second group arrangement

The second group comprises the second circulator on each output line and the SPAs. On each line, the circulator and the SPA are connected as in Figure 3.2a, exploiting an SMA connector between them.

Also in this situation it has been designed a single OFHC copper bracket where it is possible to mount the four couple of microwave devices. The bracket is shown in Figure 3.2b, has 3 mm width and it has been used a bending radius of 3 mm to bend it, respecting the empiric rule mentioned in subsection 3.1.1. Moreover both this bracket and the one for the first line of the circulators do not have a *T-connection* between the the horizontal and vertical parts of the brackets, but they have a smoother connection. This is a good practice to create more stable and less damaged copper parts and it also facilitates the workshop's work. The bracket is screwed on the upper part of the baseplate of the DR, exploiting the two holes on its horizontal part. The stability of the bracket on the plate is also ensured by two horizontal extensions of the bracket in the opposite direction compared to the one where it is possible to identify the holes.
Considering Figure 3.2c, it is possible to infer that the SPAs are screwed to the bracket using the top line of holes present on the bracket. Each of them can be screwed with four screws, obtaining a good contact with the bracket, and they need to be screwed as high as possible for the cabling design solution. The circulators are not screwed to the bracket, but they are hung to the SPAs exploiting the SMA connectors.
The input port of the circulators is connected with the circulators described in subsection 3.1.1. The third port of the circulator send the output signal to the Eccosorb filter of the ouput line and the upper port of the SPA is connected with the pump line. In this way both the pump lines and some part of the readout lines can be located above the baseplate, leading to a reduction of the number of cables below the plate.

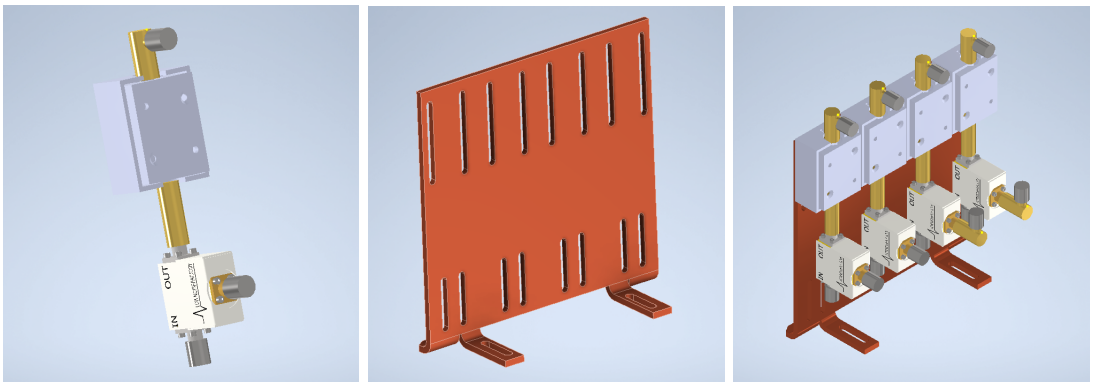

a Second group's building block. **b** Second group's bracket. **c** Second group final design.

Figure 3.2.: Figures representing the arrangement of the devices composing the second group. In figure a) and c) the SPA is represented using its packaging, the gray 2-parts box.

3.2. Thermalization

As stated numerous times in this report, it is essential that all the microwave components (concerning the project) are thermalized to the baseplate temperature. To ensure a proper thermalization, a thermal contact between the MXC plate and the electronic devices is needed.
As far as the first and the third group of electronic components are concerned, since they are all screwed to an high conductivity copper bracket which in turn is in thermal contact with the baseplate, a good level of thermalization is guaranteed.
On the other hand, considering the second group of devices, it is possible to argue that the SPAs are well thermalized but the circulators are not, since they do not touch the bracket anywhere. A way to thermalize the circulators is described in subsection 3.2.1.

3.2.1. S-shape thermalization

Let's consider Figure 3.2c. To thermalize the circulators it is necessary to find a way to create a thermal contact between them and the bracket. To achieve it, we have engineered a small OFHC copper plate with a shape resembling an S, shown Figure 3.3a, that creates the contact needed. The thermalizer is characterized by a 0.3 mm width and

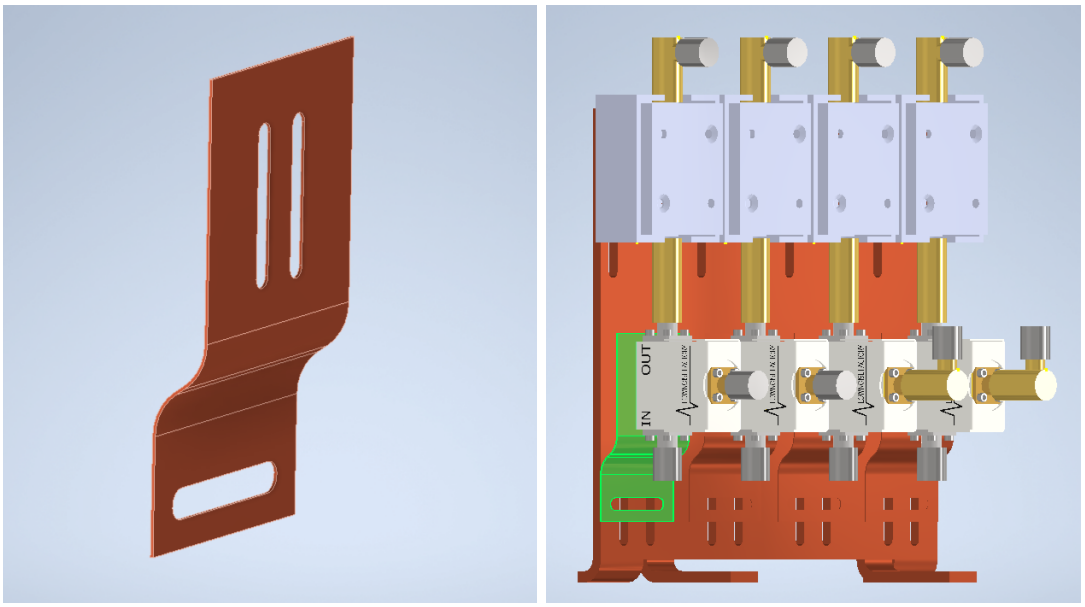

a S-shape thermalizer. **b** Second group design with thermalizers.

Figure 3.3.: a) : CAD representation of the thermalizer. b): This is the final second group's component arrangement. A thermalizer has been highlighted in green to better visualize its position.

the bending radii are such that the material is not stressed. Even if it is very thin, we believe it still guarantees a better thermalization than a copper braid. Each circulator

needs a thermalizer (for adaptability reasons), which is screwed, using two screws, to the lower holes of the bracket, as shown in Figure 3.3b. It is possible to screw a circulator to a thermalizer with four screws. It has been decided to use a thin thermalizer because, even if the distance between the circulators and the bracket should be fixed and known by the design, there could be some problems in the modelling itself or in the mounting that lead to a different *circulator-bracket distance*; since the thermalizer is very thin, it can be bent a bit by hand, compensating for the aforementioned problematic possibilities.
A 1 mm width thermalizer of the same shape has been tried, with the belief that it would have ensured a better thermalization, but, since the copper is very stiff, it was not possible to bend it by hand and, therefore, it has been discarded.
In addition, different S-shape thermalizers have been designed, and some of them could have also been good candidates to obtain a proper thermalization. The Inventor file of these thermalizers can be found in my personal folder in the *HyQu group drive*. To conclude, different thermalization solutions have been studied, in particular thermalizers characterized by different shapes compared to the S-one. A U-shape thermalizer, as example, is described in section A.2.

3.3. The setup

Combining the design ideas described in the previous sections of this chapter, it is possible to obtain the final setup that will be used in the laboratory. An Inventor picture of this is shown in Figure 3.4. In section A.4 can be found more pictures about the final setup of the baseplate of the DR. From Figure 3.4 it is possible to observe that the first and second groups of microwave components are located in the opposite part of the baseplate compared to the position of the cables and the mezzanine stage. Looking at the design, considering that all the circulators and the SPAs before the project were positioned under the baseplate, it is easy to infer that the number of RF cables below the baseplate has been highly reduced, allowing us to avoid complications during the mounting and removing of the cavities. The majority of the cables will be above the baseplate so that they, in principle, do not need to be moved until they have to be replaced, e.g. after a cable breaks. Moreover, comparing this picture to Figure A.1, it is clear that the third group of devices has been rotated by $\theta_{rot} = 90°$, reducing the length of the cables between the second circulator and the Eccosorb filter and the one between the last isolator and the mezzanine stage; furthermore, this will result also in a more ordered configuration of the cables, discussed in chapter 4. In order to accomplish this rotation and still have stable brackets, a new hole in one of the two brackets has been designed.
As final consideration, it is important to notice that all the plates used to mount the microwave devices are made of OFHC copper. This particular kind of copper reduces the number of dipoles in the plates due to the presence of oxygen, minimizing the magnetization from stray fields of the copper parts, while ensuring high thermal conductivity.

Even if this setup will be used in the DR, different design solutions have been studied

and one of them, as example, is shown in section A.5.

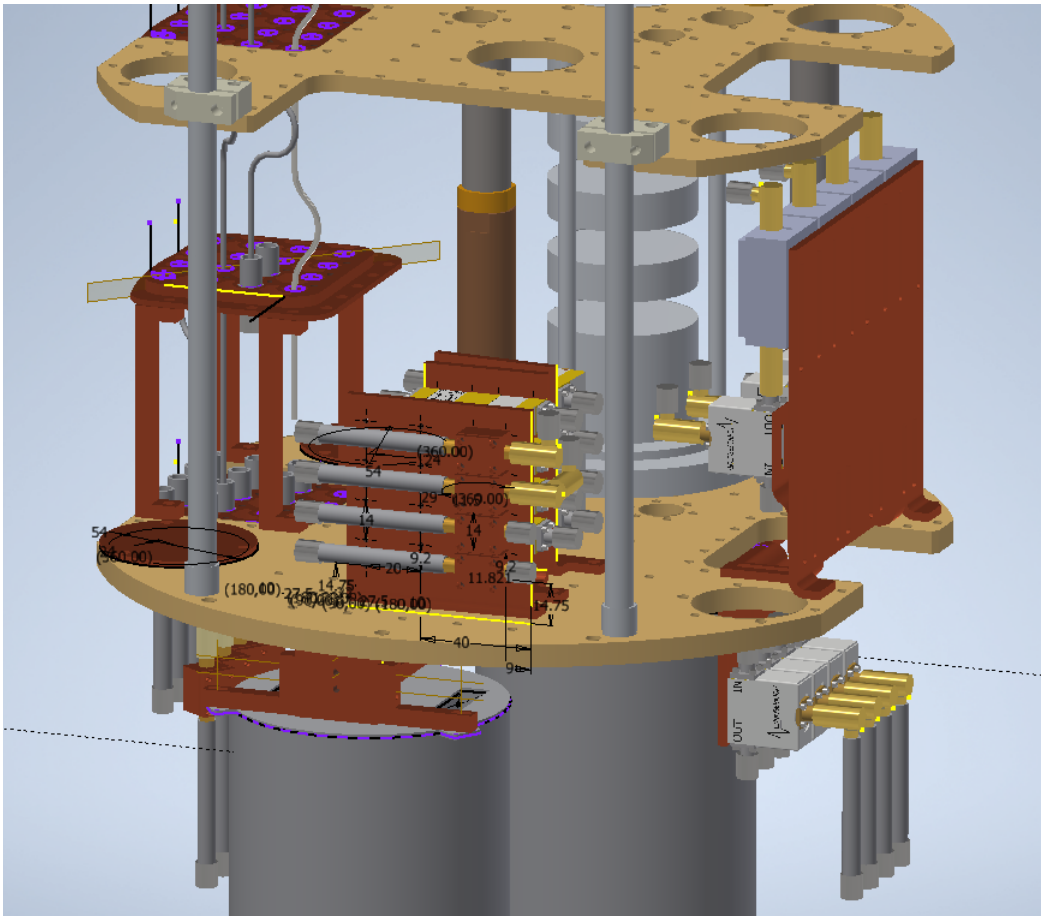

Figure 3.4.: Baseplate setup. In the picture can be identified the different devices on which the project had its focus, i.e. the circulators, isolators, filters and SPAs on the output lines. The newly designed brackets and thermalizers are also visible on the right of the figure.

Chapter 4

Cable organization

After having designed a fixed setup for the microwave components at the baseplate, as described in chapter 3, it is possible to study an efficient way to connect the different parts on the different lines with RF cables.
As stated before, the RF cables used are waveguides for electromagnetic signals and they need to properly work in the microwave regime, usually between 4 GHz and 8 GHz, since these are the typical frequencies concerning superconducting qubit experiments. The only line exploited to send signals at higher frequencies is the pump line, since the pump signal needs to be higher in frequency compared to the one we want to amplify.
The most naive justification that explains why there has been a need to think about a new wiring setup can be found in the fact that there will be inserted more microwave components and they will have a different organization compared to the one before the semester project. However, the three most important reasons that motivate a new cables' organization are:

- Reducing the number of RF cables under the baseplate of the refrigerator, permitting an easier interaction between the cavity and us.
- Finding a cables' configuration for which they can be neither touched nor moved from cooldown to cooldown, reducing the possibilities of damage.
- Having the ability to understand the cable's function from its position in the refrigerator.

To study the design possibilities regarding the cable setup, I have used Autodesk Inventor [24] and I have followed three different guidelines:

- The cables need to be as short as possible, in order to reduce the attenuation on them. For this reason the third group of microwave devices has been rotated by 90°, as explained in section 3.3.
- Different types of cables, for example a diagnostic and a pump ones, have to occupy fairly different spatial positions.
- The configuration has to seem nearly symmetric.

The second and third guidelines ensure that it will be possible to infer the cable's purpose from the location in the refrigerator. In addition, as it will be explained later in this chapter, the first guideline has not always been respected for very specific motivations.

4.1. Cable design

Before considering the design, let's look at the baseplate of the refrigerator from the point of view shown in Figure 4.1. The sixteen lines are grouped at this side of the dilution refrigerator, where it is visible the vertical structure of copper plates. The lines,

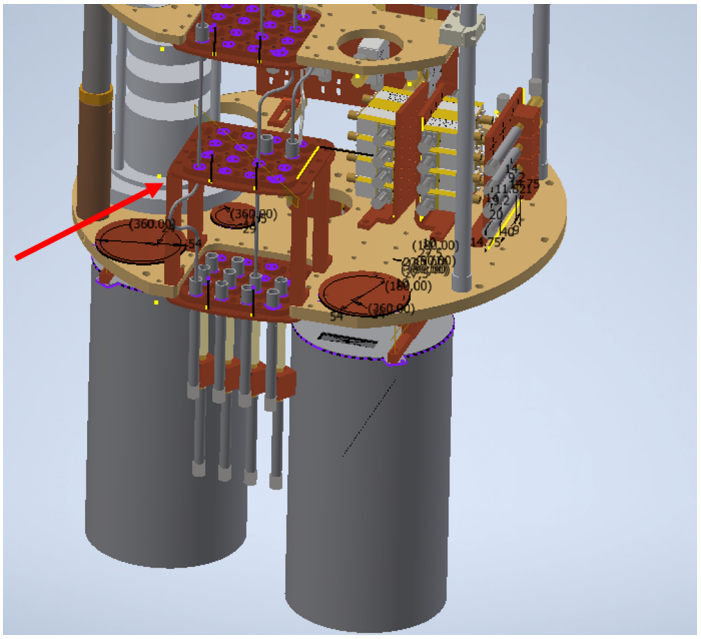

Figure 4.1.: Baseplate of the dilution refrigerator. The mezzanine stage is the copper plate above the baseplate, indicated by the red arrow.

until the mezzanine stage, are arranged in a square lattice form. The outermost row of lines comprises the input lines; they are then followed by the diagnostic lines, the pump lines and the readout lines, in this order from the external row to the innermost row. Moreover, the lines used for the first cavity are the ones on the left of the figure, while the fourth experiment exploits those on the right. In addition to this description, it is important to underline that fixed cables are used to bring the signal from the 4 K stage to either the mezzanine or the baseplate. To be more precise, the input and the diagnostic lines considered in the project start from the baseplate, the output lines arrive at the mezzanine stage. As far as the pump lines are concerned, the pump cables 1 and 2 begin from the baseplate, the other two from the mezzanine plate.

The cable design is represented inFigure 4.2. Firstly, it is possible to notice that the diagnostic lines could be shorter. It has been decided to work with longer ones such that they are spatially distant from the cavities. Secondly, it has been taken into account that two pump lines start at the MZ plate and the other two at the baseplate. Moreover, this figure can be compared with Figure 2.5 to verify that all the necessary connections are present. The bends on the individual cables are designed to be mostly 90° because they

are easier to achieve in practice, even if they will lead to increase the length of a cable, obtaining a better match between the design and the real implementation.

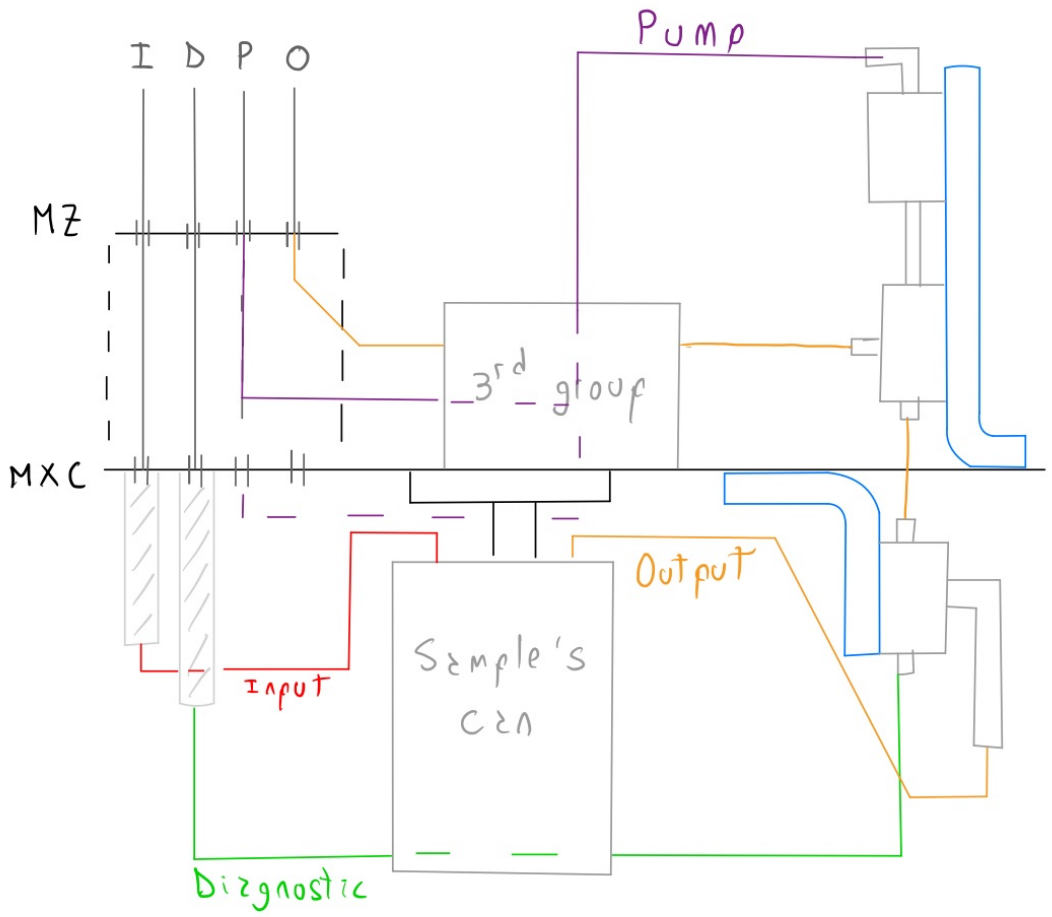

Figure 4.2.: Schematic of the design of one entire set of lines. The same naming convention as in the main text has been used.

Concluding, it is possible to count that for each set of lines we need seven different cables; a more precise visualization of them is reported in section B.2 and the naming convention of the cables used from now on is described in section B.1.

4.2. Cable properties

Each cable designed, once made in the laboratory, needs to satisfy specific properties, e.g. it must not to attenuate the signal too much, in order to be useable in our experiments.

The first attribute used to describe a cable is its length. To each cable a specific value of length and a tolerance on that value is assigned, such that the cable can still be used in the refrigerator. The length of the cable follows from its length on the design and the process that I have used to calculate it is described in section B.3. The following table reports the cables' lengths:

Cable lengths [mm]				
	Line 1	Line 2	Line 3	Line 4
IS	292.0 (2.0)	306.0 (2.0)	264.0 (2.0)	252.0 (2.0)
SC	321.0 (2.0)	366.0 (2.0)	390.0 (2.0)	344.0 (2.0)
CC	81.0 (1.0)	70.0 (1.0)	70.0 (1.0)	81.0 (1.0)
CE	225.5 (2.0)	191.0 (2.0)	142.0 (1.0)	135.0 (1.0)
IR	134.0 (1.0)	117.0 (1.0)	102.5 (1.0)	94.5 (1.0)
DKC	441.0 (2.0)	441.0 (2.0)	441.5 (2.0)	428.5 (2.0)
PPS	398.5 (2.0)	391.5 (2.0)	341.5 (2.0)	354.5 (2.0)

Table 4.1.: Table that summarizes the lengths of the 28 cables designed for the experimental setup in the refrigerator. The length is given in mm and the quantity reported in the bracket is the tolerance to be considered when actually making the cables

Another important decision that needs to be made when making the cables is whether to use normal connectors or non-magnetic connectors. As a rule of thumb, normal connectors should always be used, unless the presence of specific constraints, since they are cheaper and the soldering process is easier, leading to usually better scattering parameters of the cable. In our case, we need to avoid flux noise on the sample. Since the cavity is inside a magnetic shield, the only cables that could lead to magnetic noise near the device are the ones directly connected to the cavity, i.e. IS and SC. For this reason, the connectors inside the magnetic shield need to be non-magnetic; for the cables' ends outside the shield it is possible to use a normal connector. For all the other cables only normal connectors are used.

The other important parameters of the cables are the reflection coefficients at each port and the transmission coefficient of the cables and they can be defined using the scattering matrix for a multiport circuit:

$$S_{ij} = \left.\frac{V_{out,i}}{V_{in,j}}\right|_{V_{in,k}=0 \ \forall \ k \neq j} \tag{4.1}$$

For our cables, since they only have two I/O ports, S_{11} and S_{22} are the reflection co-

efficients respectively at port 1 and 2, and $S_{21} = S_{12}$ is the transmission coefficient of the cable. The reflection and transmission coefficients take into account the quality of the cable's preparation, considering also the soldering process of the connectors to the cable. Moreover, longer cables should in principle have lower S_{21}. Excluding from the following discussion the pump cables, the signals used in the experiment have usually low intensities and, for this reason, the transmission of the cables needs to be as high as possible to have good results. Since the signals used are in the 4-8 GHz regime, it should be sufficient to study the scattering parameters in the 3-10 GHz range, but we decided to collect the data in a larger range, namely 0-12 GHz; this is a further insurance of the quality of the cables. All the cables, besides the ones that transfer the signal from the cavity to the SPA (SC and CC), need to respect these two conditions:

- $S_{21} > -1$ dB for frequencies below 12 GHz.
- $S_{11} < -20$ dB & $S_{22} < -20$ dB for frequencies below 12 GHz.

Considering now the SC and CC cables, since the output signal from the cavity is very low due to the fact that there is a low number of excitations in the cavity, we use stricter conditions, i.e. the reflection coefficients need to be below -23 dB in the frequency range considered. If these work's conditions are satisfied, we have obtained a good trade-off between our ability to prepare a cable and the fact that a cable does not sufficiently attenuate the incoming signal to invalid the experiment and the connectors do not behave as bottlenecks for the signal.
As far as the pump cables (PPS) are concerned, they have to be treated in a bit different way since the pump signal has a frequency around 17 GHz and it is possible to increase its power without affecting the experiment. For these reasons, we study the spectrum of the scattering parameters in the 0-20 GHz range and the boundary conditions for the scattering parameters can be less strict; nevertheless we try to have cables that follow the limitations reported in the previous list.

4.3. Cable measurements

In this section I report only the measurements of the scattering parameters regarding the IS cables, that I will use as an example for all the other cables for the baseplate of the DR. All the other measurements and the respective results are shown in section B.4. The reference measurement for the IS cables can be found in subsection B.4.1. The results are shown in Figure 4.3. First of all it is possible to notice that the noise seen in the reference measurement, shown in Figure B.2, in the transmission is also present in the transmission of these cables, at high frequencies. Following the guidelines defined in section 4.2 to evaluate the possibility to use a cable, it is clear that IS-2 cannot be considered a good cable, since its transmission is characterized by a dip near 8 GHz and the reflection from both ports at nearly the same frequencies is much higher than -20 dB. To analyze the other cables, since they respect more or less the baseline, it is necessary to introduce a table of important values in the 0-12 GHz regime. From Table 4.2 it is possible to see

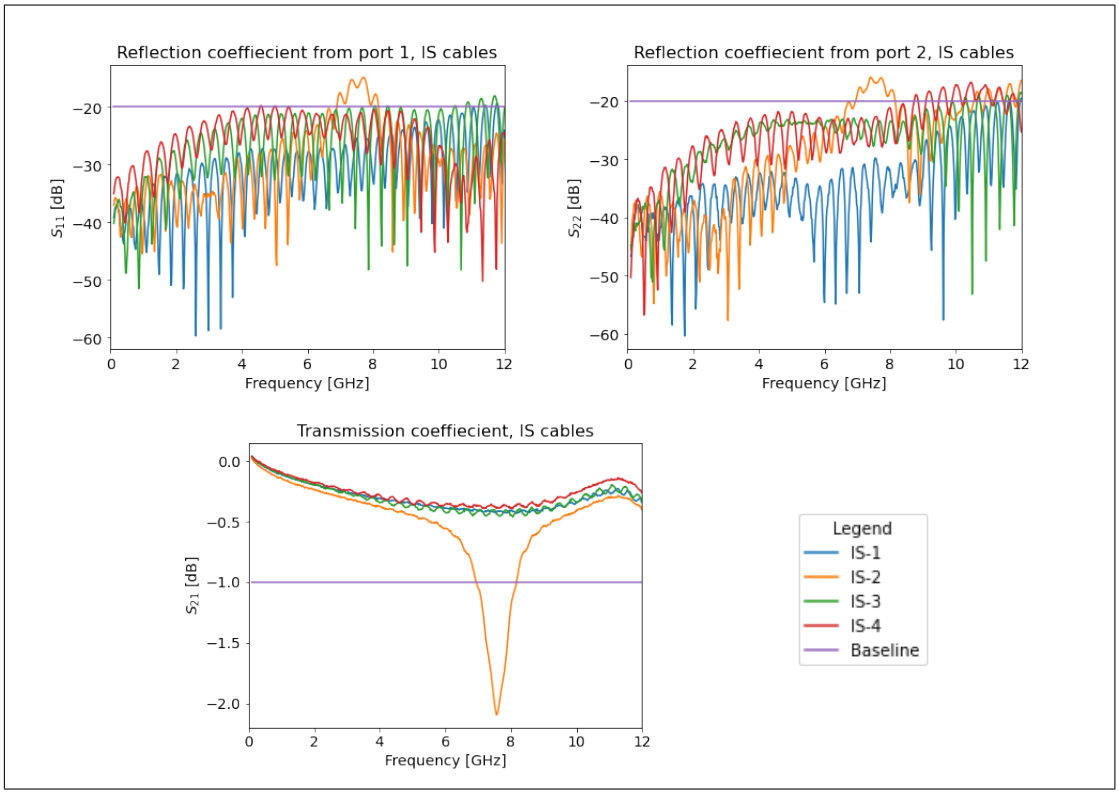

Figure 4.3.: Transmission and reflection coefficients of all the IS cables. In the upper plots it is possible to see S_{11} and S_{22}, in the lower one S_{21}. In each plot is present the baseline line, used to determine the quality of the cables.

Critical values of the scattering parameters [dB]			
Cable	Max S11	Max S22	Min S21
IS-1	-19.4	-19.6	-0.4
IS-2	-14.9	-16	-2.1
IS-3	-18.1	-18.6	-0.5
IS-4	-19.8	-16.8	-0.4

Table 4.2.: Critical values for each cable. The measure's unit is in dB.

that the only cable that might satisfy our requirements is IS-1, since IS-3 and IS-4 have too high reflection coefficients. IS-1 is a good cable since it does not respect the baseline just above 10 GHz, but these frequencies are also characterized by some problems in the reference measurement. As last consideration, the cable IS-2 has to be remeasured since

different measurements taken by different group members have shown to be inconsistent to what I have measured.

Chapter 5

Conclusion

The main goal of the semester project was to design a new setup and wiring configuration for the MXC plate of the aforementioned dilution refrigerator. This was necessary to have the possibility to integrate two additionally SPAs and to have a ordered cabling scheme.
The goals, at least from the design point of view, have been achieved. Nevertheless, as far as now, we have tried to mount the setup just using two RF cables as a test. The test has yielded positive results and, thanks to this, I am confident there should not be any problems when the entire setup will be mounted in the refrigerator. The only complications that might arise in that moment can derive from an imprecise length of the cables or from possible inaccurate bendings of the cables.

The new baseplate setup has been described in chapter 3. As far as the brackets are concerned, we already have them in the laboratory, ready to be mounted in the DR after proper cleaning. Considering the thermalizers, we asked the Physics' Workshop to prepare one of them as a test and it worked as expected. In this way, having chosen the right width of the thermalizers for our purposes, every componenent in the setup can be properly thermalized.

In chapter 4 the new cabling design for the baseplate of the refrigerator has been shown. The properties used to define a good cable have also been described in that chapter. The cables have been prepared by each member of the Gandalf team and they cannot be properly tested because we still have problems in the calibration of the VNA. Nevertheless, it has been possible to decide which cables should have been discarded. As it follows from chapter 4 and Appendix B, it is possible to say that we now have 15 good cables out of the 28 needed. However, a final decision on which of the 15 cables can be used in the experimental setup has yet to be made. For this reason, we need to continue preparing some cables and be ready for the next cooldown of the refrigerator, probably in July 2022.

To conclude, the setup designed during this project can be extended to be used in other DRs with similar experiments, in order to have a smarter organization of the baseplate components. The adaptation to other DRs is possible if they have approximately the same size of our refrigerator and if the requirements, considering the number of lines and the collocation of the experiments, are similar to ours. A way to obtain a better design solution would be to have all the pump cables starting from the mezzanine stage and not from the baseplate.

Appendix A

Chapter 3, Supplementary Information

A.1. Third group's arrangement before the project

In Figure A.1 is shown the disposition and the location of the third group of microwave components (section 3.1). At the left of the image it is possible to see the mezzanine stage (copper plate between the two refrigerator's plate). The third group's component are on the baseplate, thermalized to it using OHFC copper brackets. They can be identified looking at the space above the MXC plate, in the front of the picture. They are connected in series from input to output of the group and they are one Eccosorb filter, one K&L filter and two isolators for each line.

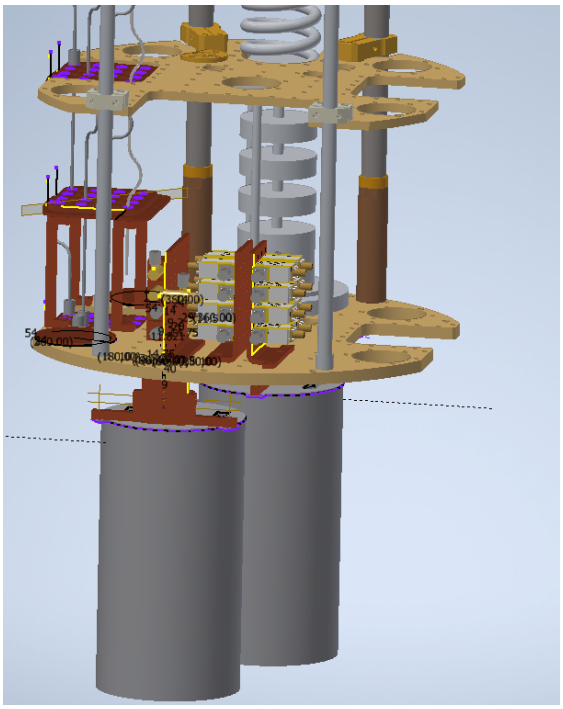

Figure A.1.: Third group's devices lie on the baseplate, in the middle of it (as seen from the image).

A.2. U-shape thermalization

In Figure A.2 is shown a thermalizer with a form resembling an U. This particular one would have been a thermalizer for all the four circulators, since all of them can be screwed to the two parallel horizontal holes. It would have been made of OFHC copper and it would have had a width of 1 mm. Moreover, considering this design, it could have been directly screwed on the upper line of holes in Figure 3.2b. It has been discarded for two reasons:

- The bending radius would have been very small, putting a lot of stress on the metallic sheet. In addition to this, the workshop only has machinery that ensure a

precise bending up to a bending angle $\theta_{bending}^{max} \approx 100°$.

- It would have been necessary to design another big hole on the back of the thermalizer to have the possibility to screw the circulators, but the screwing would have remained very challenging.

Figure A.2.: U-shape thermalizer. It is an example of a different thermalization solution compared to the one presented in subsection 3.2.1

A.3. Drawings for the workshop

After having designed the new OHFC copper parts, they were sent to the workshop exploiting a step file and a drawing of the part. The *Physics' Workshop* built the corresponding part. The drawings sent to the workshop are shown in Figure A.3, Figure A.4 and Figure A.5

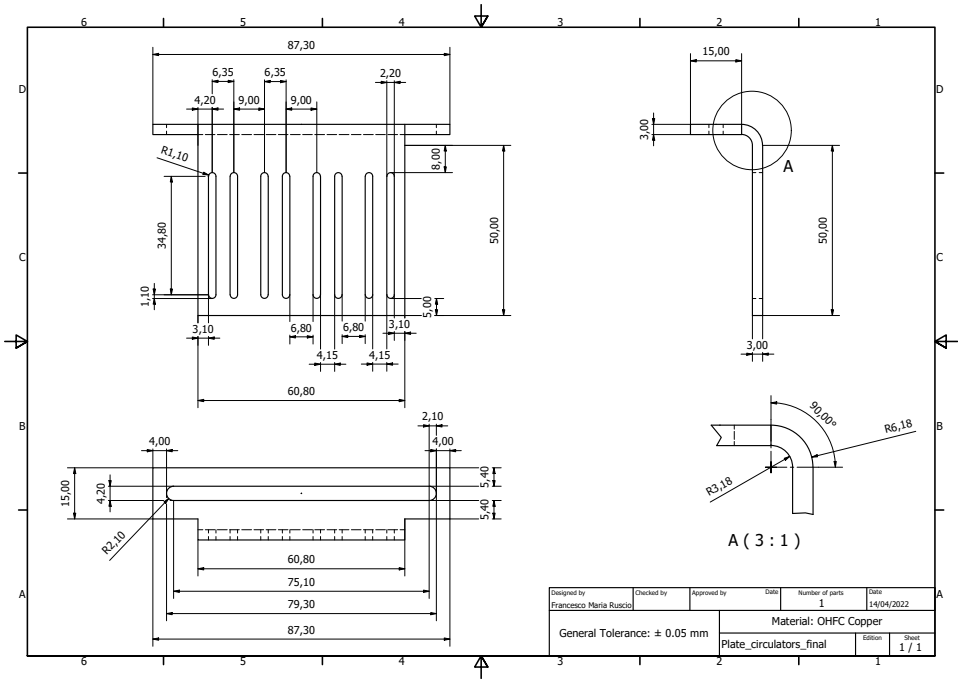

Figure A.3.: Drawing of the bracket for the first line of circulators, described in subsection 3.1.1.

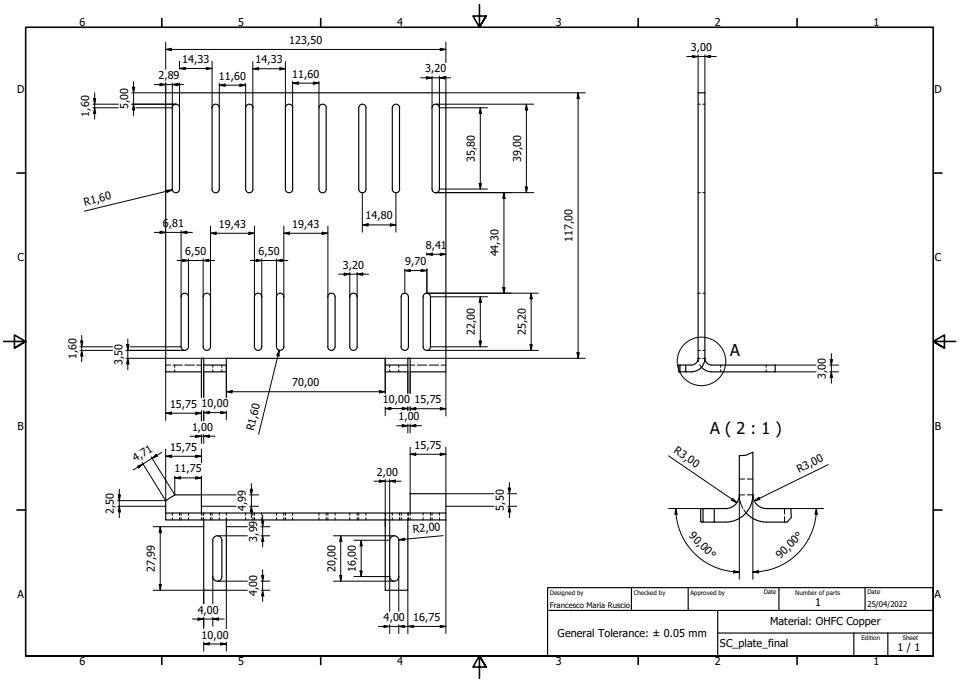

Figure A.4.: Drawing of the bracket for the second group of devices, described in subsection 3.1.2.

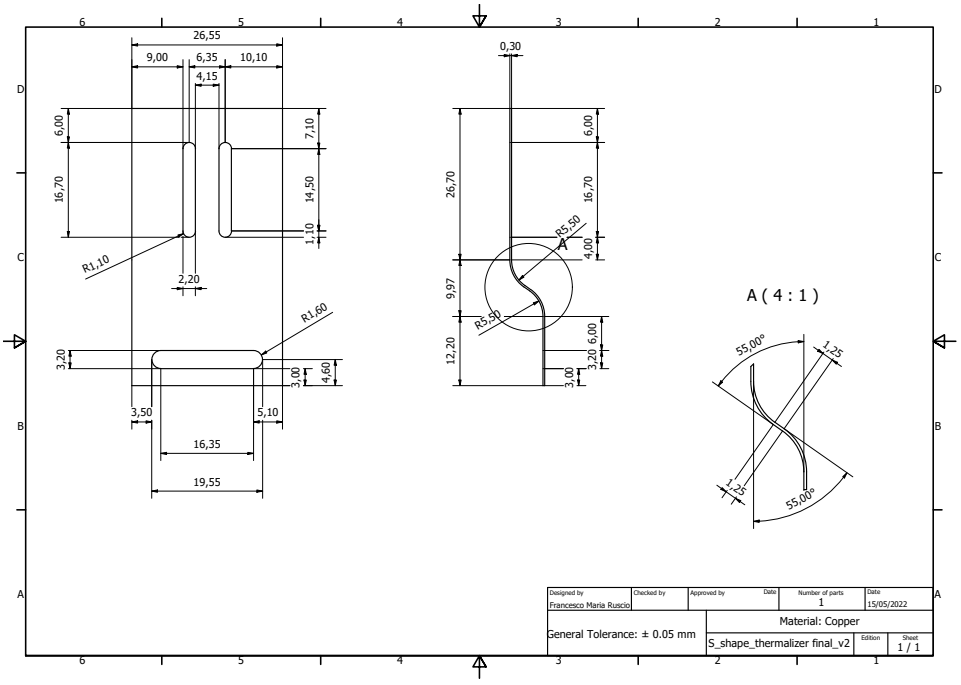

Figure A.5.: Drawing of the S-shape thermalizer, described in subsection 3.2.1

A.4. Final setup, additional pictures

Additional images describing the final setup mounted in the DR are shown in Figure A.6. A comprehensive image of the DR is in Figure A.7.

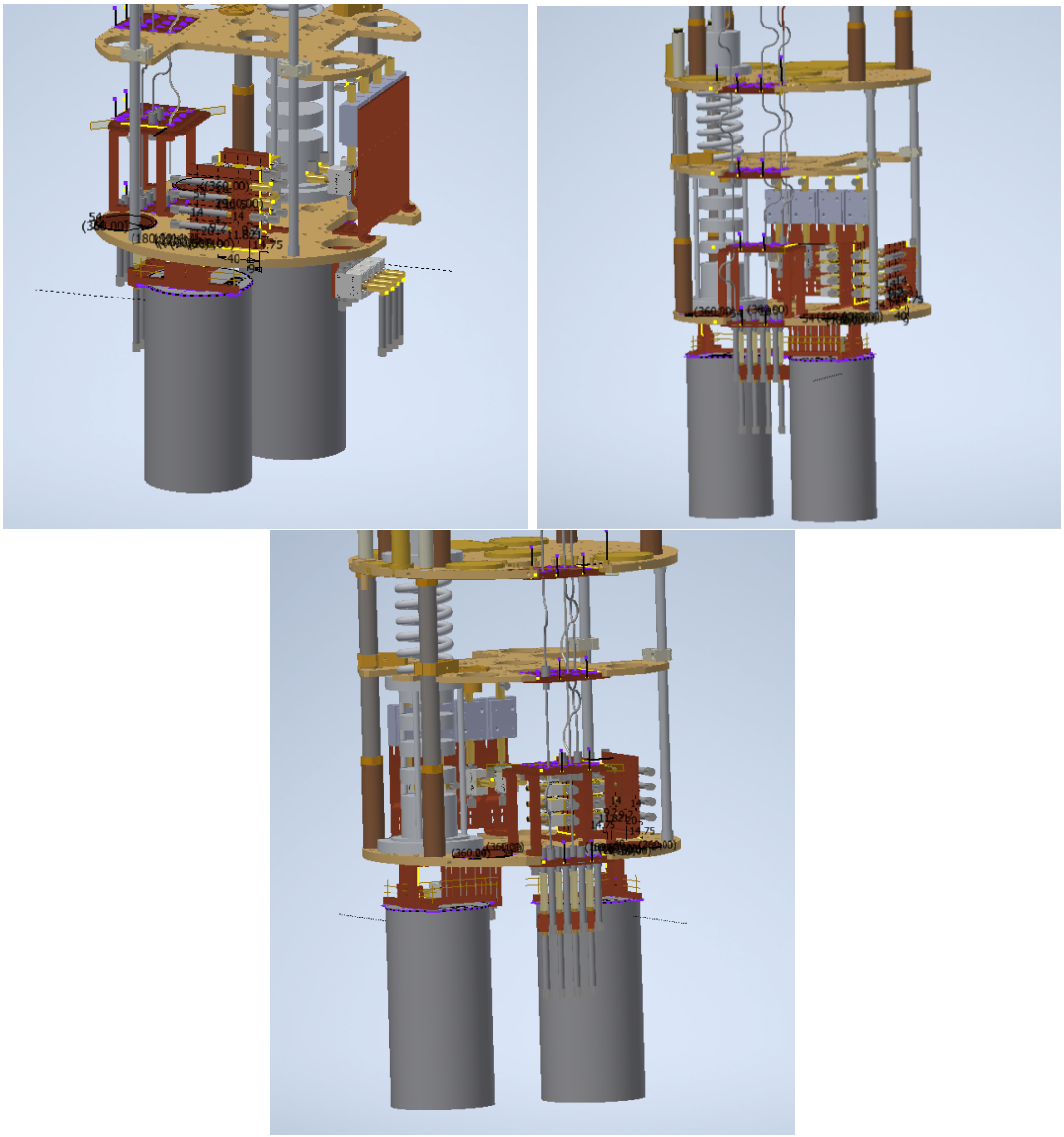

Figure A.6.: Images from different point of views of the baseplate setup.

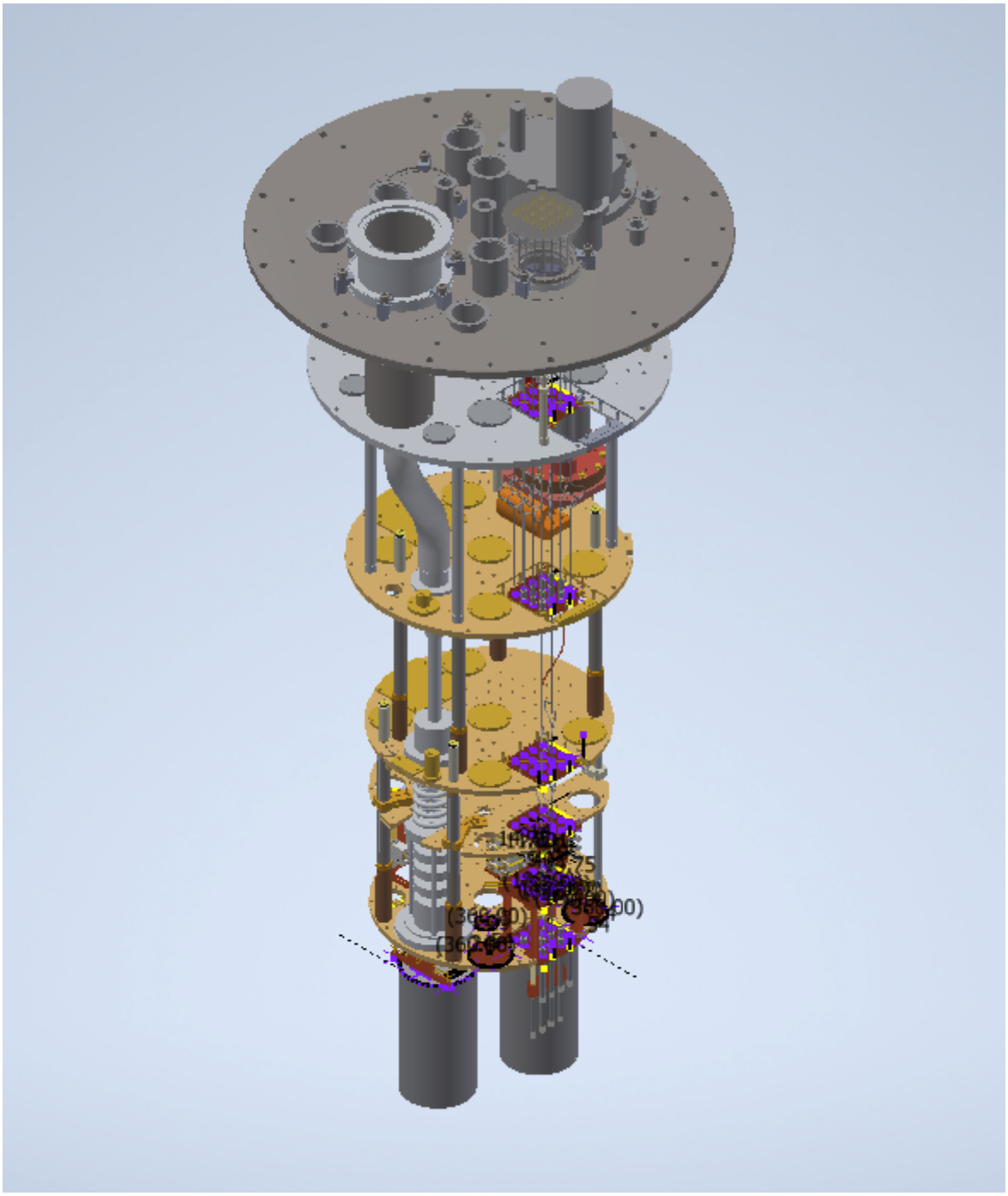

Figure A.7.: DR in Inventor.

A.5. Alternative setup

An example for a different design solution compared to the one in section 3.3 is shown in Figure A.8. In this case the third group of devices has not been rotated and the first two groups of devices are different, because the second one comprises only the SPAs. Having both circulators of the output line below the baseplate, there would have been more RF cables under the baseplate, not permitting us to achieve one of the goal of the design of the new baseplate setup listed in chapter 3. With this design, the two circulators would have been connected by an SMA and the connection between the SPAs and the circulators would have been accomplished by cables. As final consideration, exploiting this setup, it would have not been necessary to design thermalizers since all the different microwave components are attached to a bracket.

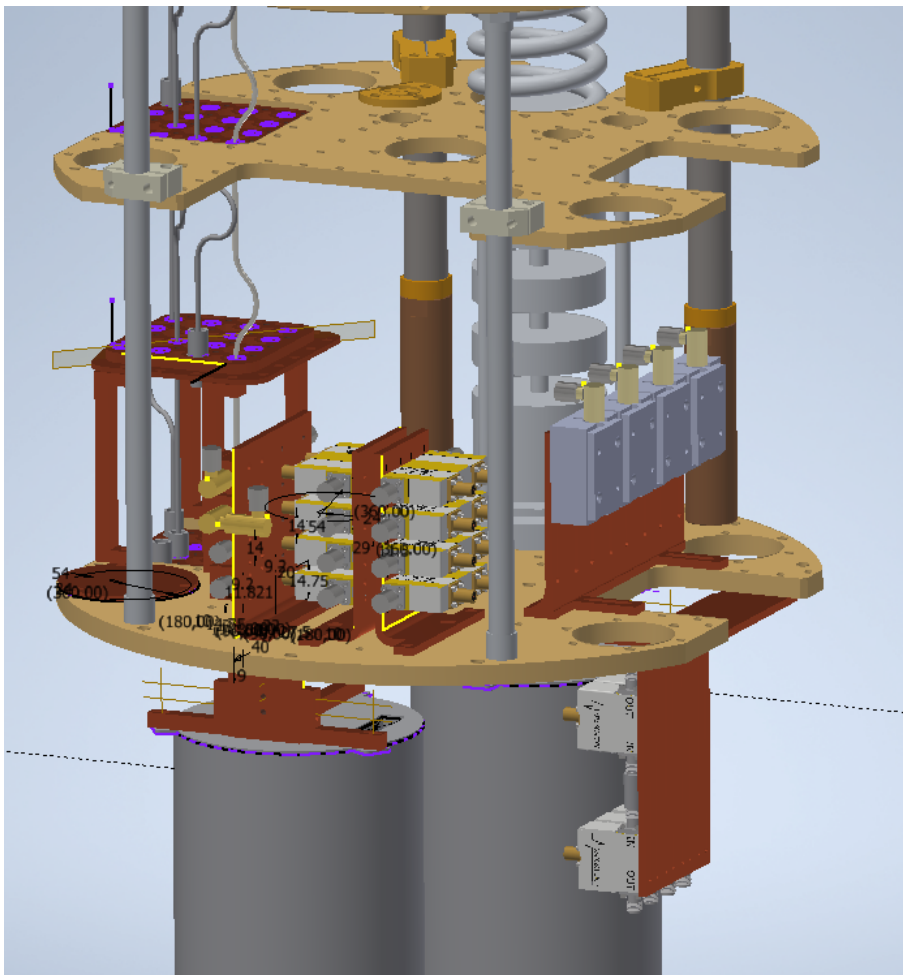

Figure A.8.: A possible alternative baseplate setup.

Appendix B

Chapter 4, Supplementary Information

B.1. Cables' naming convention

As mentioned in section 4.1, seven different RF cables need to be designed for each experiment. Referring to Figure 4.2, the following names have been chosen for the cables:

- IS : from Input line at the baseplate to the Sample
- SC : from th Sample to the first Circulator on the output line
- CC : from the first Circulator to the second Circulator on the output line
- CE : from the second Circulator to the Eccosorb absorber on the output line
- IR : from the last Isolator on the output line to the Readout line at the mezzanine stage
- DKC : Diagnostic line, from the K&L filter to the first Circulator on the output line
- PPS : Pump line, from the Pump line to the SPA.

Then, a cable "XX" belonging to the experiment number "#" is called "XX-#"; for example, if we consider the input cable for the third cavity it will be "IS-3". Another example of the naming convention for the cables can be found in Figure B.1.

B.2. Cable design, additional images

Here I report pictures for the entire set of cables needed for the fourth experiment. Each cable can be identified as a broken line in the Inventor environment modeling the refrigerator. I have tried to minimize the length of the cables, even if it is not possible for each cable because there are other constraints. In addition, it is possible to check that right turns of the cables have been preferred . The only cables that are located near the cavities are the IS and the SC ones, leading to a large decrease of the number of cables in that area. Finally, each cable has a very precise spatial location that permit to distinguish it from the others.

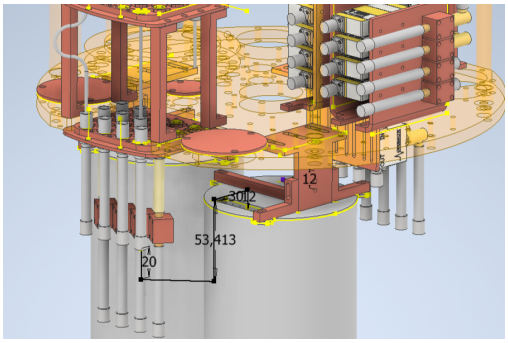

a IS-4

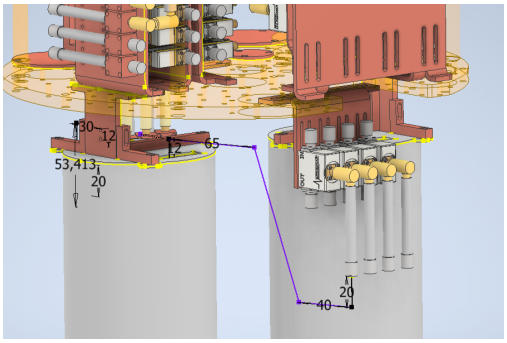

b SC-4

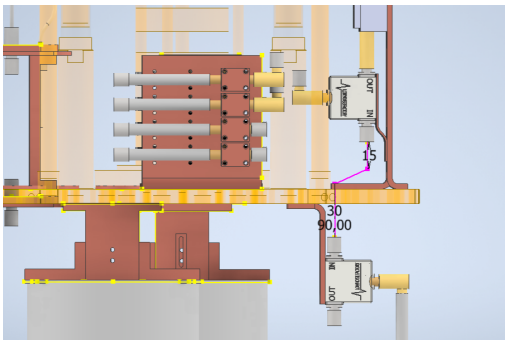

c CC-4

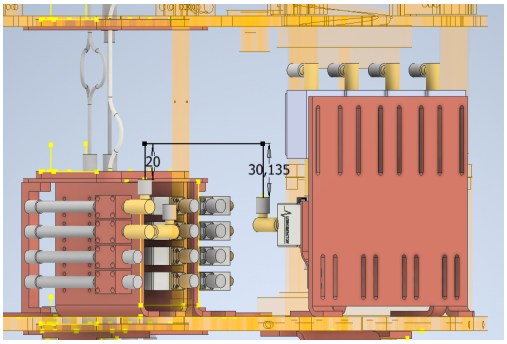

d CE-4

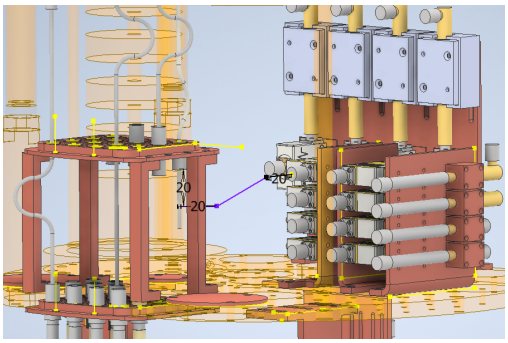

e IR-4

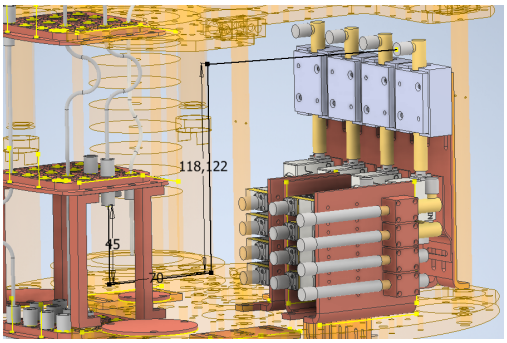

f PPS-4

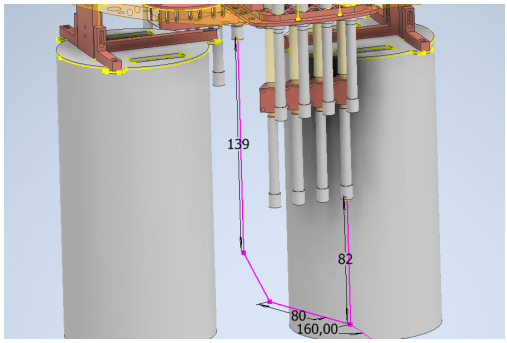

g DKC-4

Figure B.1.: Cables used for the fourth experiment.

B.3. Cables' length evaluation

The procedure used to obtain the lengths of the cables, shown in Table 4.1, is the following:

1. Measure the length of the cable designed in Autodesk Inventor, called $L_{inventor}$. Since the design is very precise, the length will have a precision of 1 μm. The decimal part of the number is called "d". For example, if $L_{inventor} = 94.678$ mm, it will be $d = 678$.

2. Approximate $L_{inventor}$ such as:

$$\begin{cases} L_{approximated} = \lceil L_{inventor} \rceil \ if \ d > 200 \\ L_{approximated} = \lfloor L_{inventor} \rfloor \ if \ d < 200 \end{cases} \tag{B.1}$$

3. For this point consider only SC and IS cables. On inventor they are only designed until the entrance of the sample can, but they are longer since they need to be plugged in the cavity ports. This additional length, $L_{additional}$, has been estimated and needs to be summed to $L_{approximated}$, updating its value.

4. It is now necessary to account for the fact that the inventor cables are 2D cables, but in the refrigerator will be used 3D cables. To be sure that this is not a problem, to each cable length will be summed an L_{extra} and the final cables will be characterized by $L_{practice}$ such that:

$$L_{practice} = L_{approximated} + L_{extra} \tag{B.2}$$

   L_{extra} follows directly by the presence of two different parts on a cable:

   - Connectors: straight connections contributes to L_{extra} with 0.5 mm, the other ones with 1 mm.
   - Turns: each straight angle turn contributes to L_{extra} with 1 mm. For soft turns (at most 40°) the contribution is 0.5 mm, for hard ones (much more than 90°) we consider an additional length of 1.5 mm.

It is clear from the previous discussion that the length of each cable has been probably overstimated; this ensures that the cable is not too short during the mounting. Actually, the mounting of some cables has been already tested, leading to the expected results and, for this reason, I believe that this way to estimate the length of the cables is correct.
The tolerance on the length of each cable shown in section 4.2 has been decided such that if the length of the cable can be measured by the caliber the tolerance is 1 mm and otherwise is 2 mm.

B.4. Cable measurements, complementary

B.4.1. Reference's measurements

Each cable is measured using a VNA, *Vector Network Analyzer*. Before the measurement, the VNA needs to be calibrated. This is necessary because to access the scattering parameters of a target cable, we need two extra cables to measure it and the calibration takes in account also their presence. After having properly calibrated the VNA, the measurement of a single SMA connector should yield a transmission near to 0 dB and reflection coefficients very low, since the connector has been industrially designed and optimized to obtain so. I call reference measurement the measurement of the single SMA connector. This reference, used for all the other measurements except the pump cables' ones, is shown in Figure B.2. The figure shows clearly that there are some

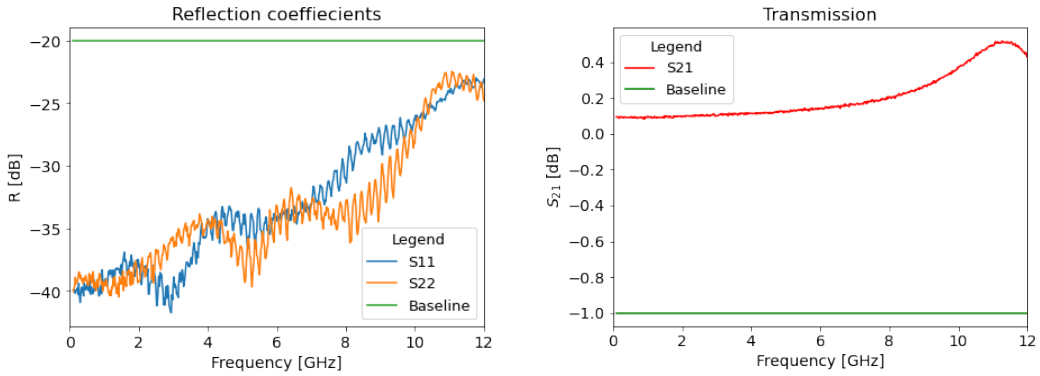

Figure B.2.: Reference measurement for IS, SC, CC, CE, IR, DKC. Reflection and transmission coefficients for a single SMA connector are shown.

problems during the calibration due to a malfunction in the calibration kit. Considering the reflection coefficient it is possible to notice a large increase for frequencies higher than 8 GHz; nevertheless since the maximum value reached by the reflection coefficients is nearly -23 dB, this calibration problem should not invalidate the measurement of the reflection parameters of the IS, CE, IR, DKC cables, i.e. the cables that need to have reflections lower than -20 dB. On the other hand, SC and CC cables cannot be properly measured. As far as the transmission coefficient is concerned, it is clear that is higher than 0 dB and this means that the connector should amplify the signal, an impossible fact since it is a passive component. However, the transmission coefficients of the cables can still be studied because this noise on the transmission is very low, reaching at most 0.5 dB. In conclusion, to have indisputable measurement, we should look for auxiliary cables that do not yield to these problems.

B.4.2. CE, IR, DKC measurements

In this subsection are summarized the analysis for the cables that need to guarantee reflection coefficients lower than -20 dB until 12 GHz. IS cables are not considered since they have been already analyzed in section 4.3. All the measurements can be found in the next figures.

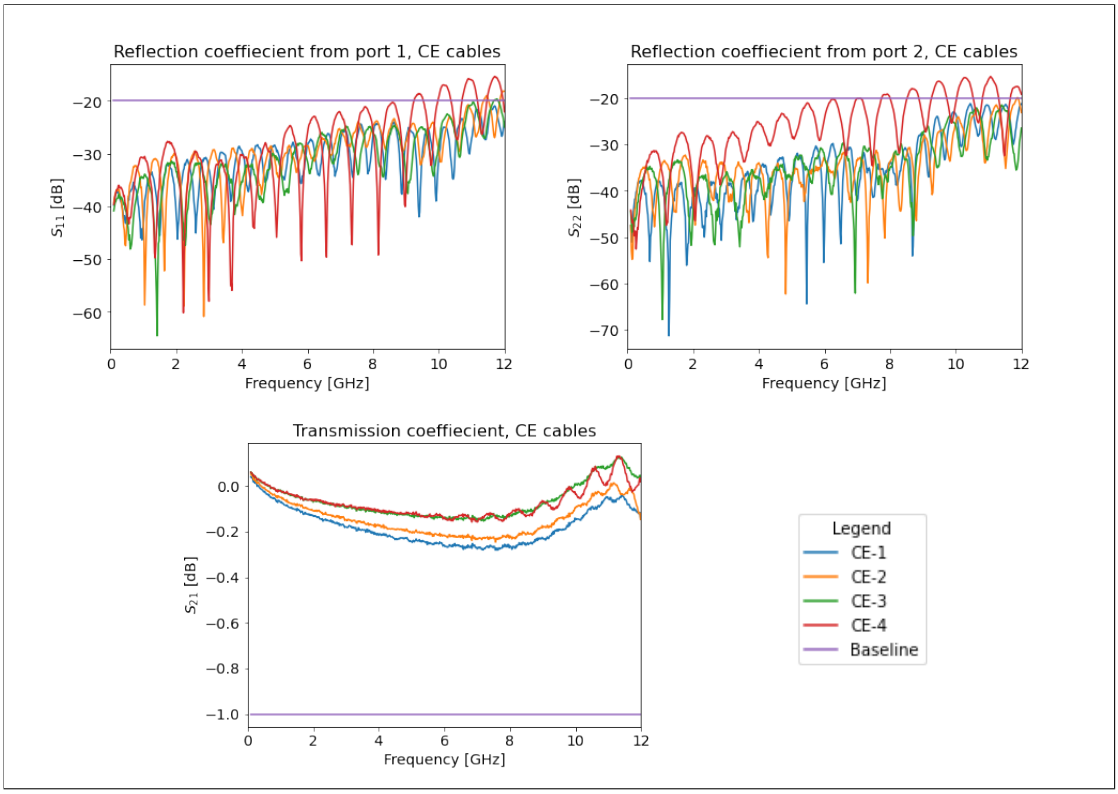

Figure B.3.: Transmission and reflection coefficients of all the CE cables.

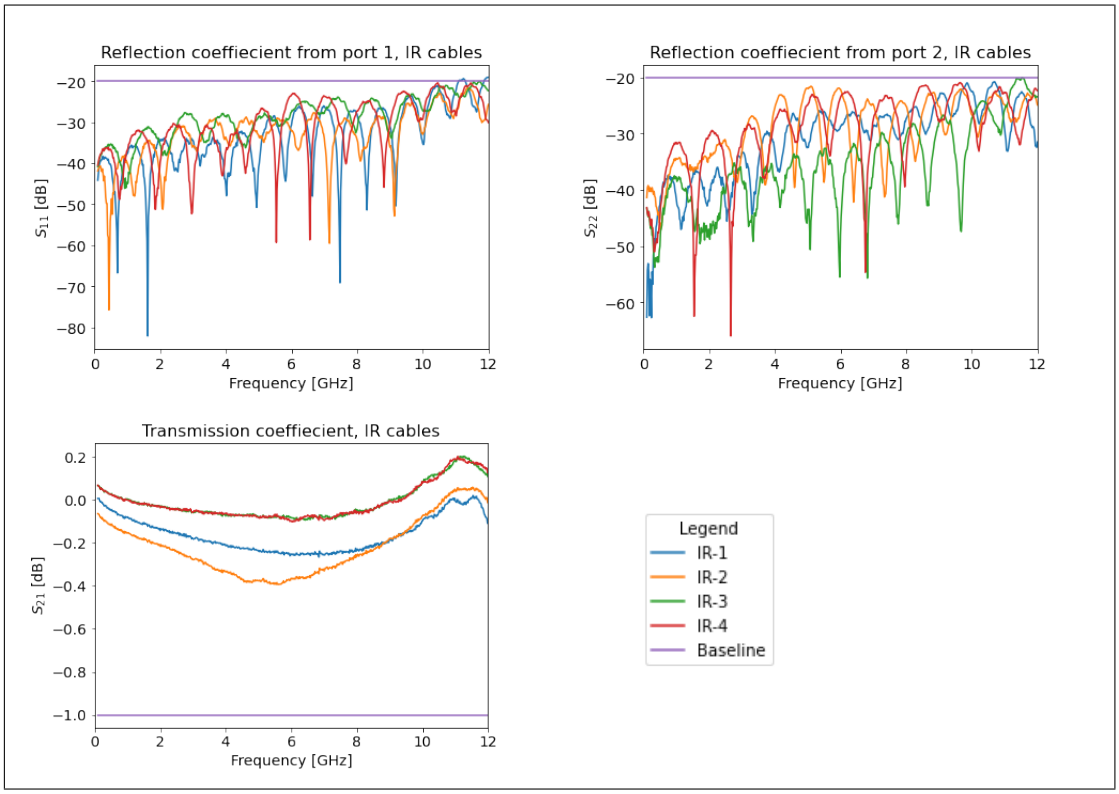

Figure B.4.: Transmission and reflection coefficients of all the IR cables.

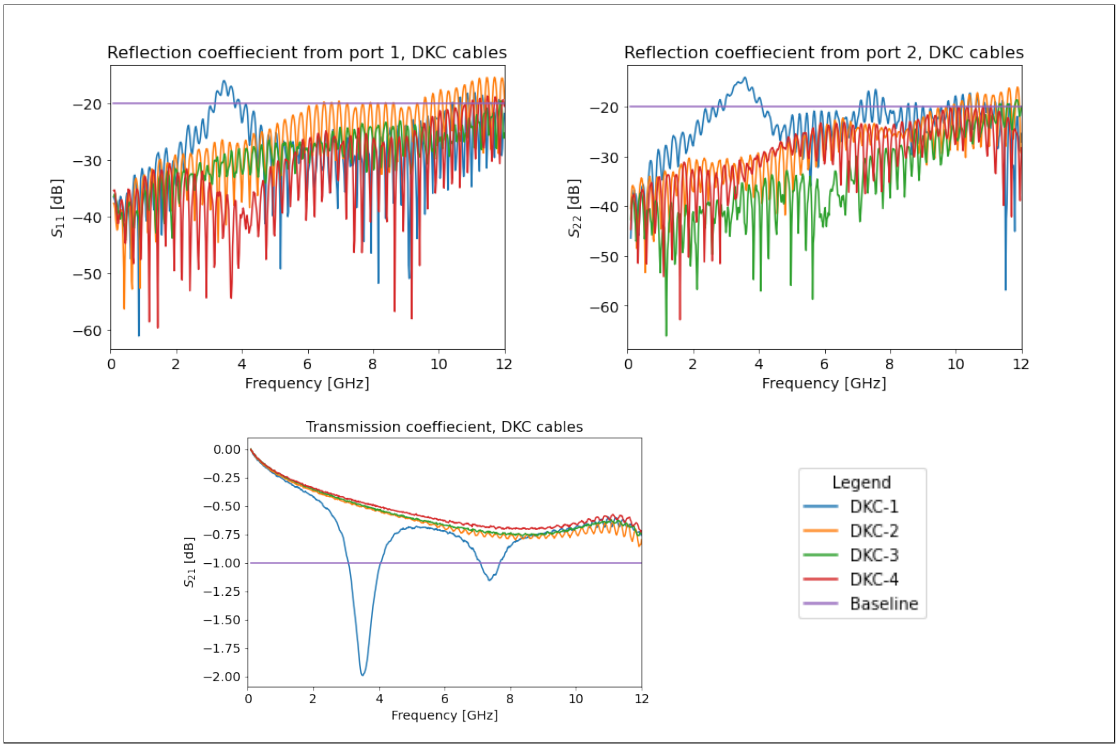

Figure B.5.: Transmission and reflection coefficients of all the DKC cables.

To have a more precise evaluation of the cables, it is also important to report a table for the critical values of the scattering parameters (Table B.1).

Let's consider CE cables. They are all characterized by very high transmission coefficients. As far as the reflection is concerned, only CE-1 respects the baseline; however also CE-2 and CE-3 are good cables since their reflection coefficients exceed the baseline only at high frequencies, where we might have had problems during the calibration process. CE-4, on the other hand, has to be discarded because its reflection coefficients are very high for a broader range of frequencies.
As far as the IR cables are concerned, they can all be considered good cables.
Finally, considering DKC cables, they have lower transmission coefficients since they are longer. It is clear that DKC-1 is not a good cable, both from the its critical values of the scattering parameters and its spectral behaviour. Also DKC-2 has to be discarded since its reflection coefficients assume values too high if compared to the baseline. DKC-3 and DKC-4 can be considered good cables.

Critical values of the scattering parameters [dB]			
Cable	Max S11	Max S22	Min S21
CE-1	-21.0	-21.2	-0.3
CE-2	-18.2	-20.0	-0.2
CE-3	-19.7	-21.5	-0.2
CE-4	-15.4	-15.4	-0.2
IR-1	-19.0	-20.8	-0.3
IR-2	-21.6	-21.6	-0.4
IR-3	-20.1	-20.1	-0.1
IR-4	-20.4	-21.0	-0.1
DKC-1	-16.0	-14.1	-2
DKC-2	-15.4	-16	-0.9
DKC-3	-19.6	-18.7	-0.8
DKC-4	-18.7	-19.8	-0.8

Table B.1.: Critical values for each cable. The measure's unit is dB.

B.4.3. SC, CC measurements

As stated before, the measurements of the reflection and transmission coefficients of the SC and CC cables could be not valid, but I still illustrate them here for sake of completeness. The results are reported in the following figures and table.
Firstly, we have just prepared one CC cable, due to the calibration problem. Considering the only one we have, the transmission is very high since the cable is very short. Moreover, the reflection coefficients are very good until 10 GHz but they cannot be quantified in a correct way since they approach the value of the reference measurement. The only problem that CC-2 shows is that S_{11} increase a lot after 11 GHz. It is not clear if this is a cable to discard because it is overall very good, and for this reason it is difficult to prepare one that is better, and probably it has a problematic feature at frequencies we are not anymore interested in for our experiments.
As far as SC cables are concerned, as it is possible to see from Table B.2, they should all be discarded since the reflection coefficients are extremely high compared to the baseline and the reference.

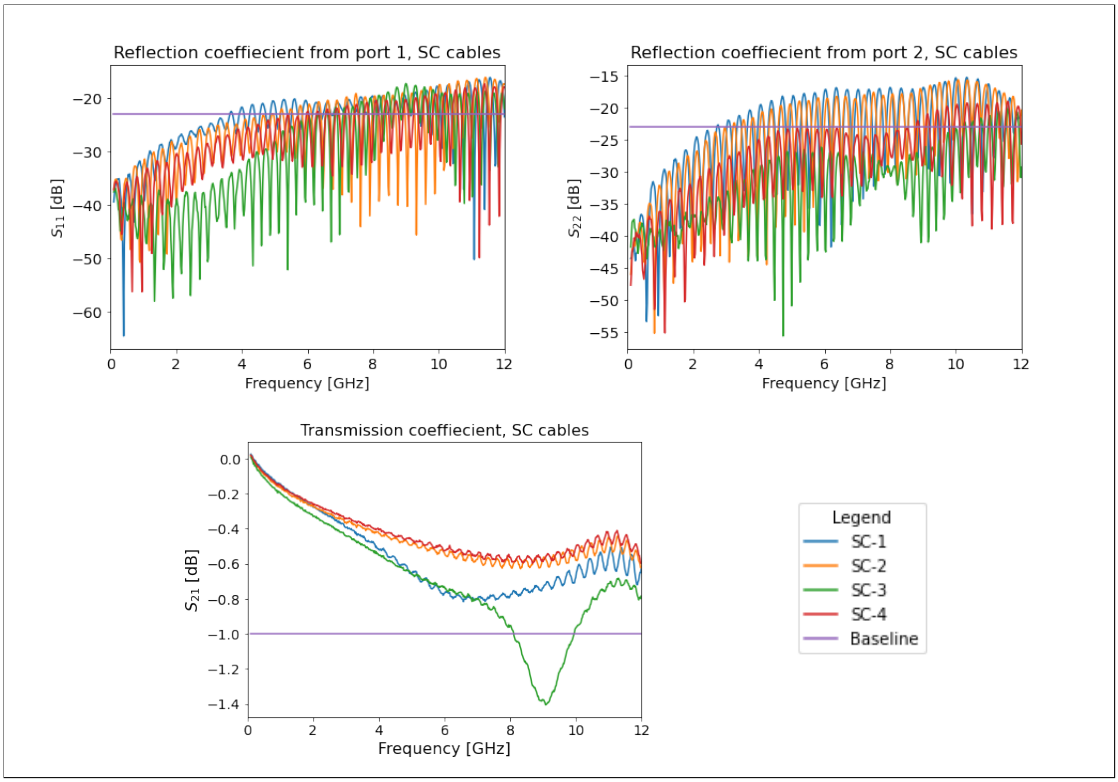

Figure B.6.: Transmission and reflection coefficients of all the SC cables. It is important to notice that the baseline for the reflection coefficients is -23 dB.

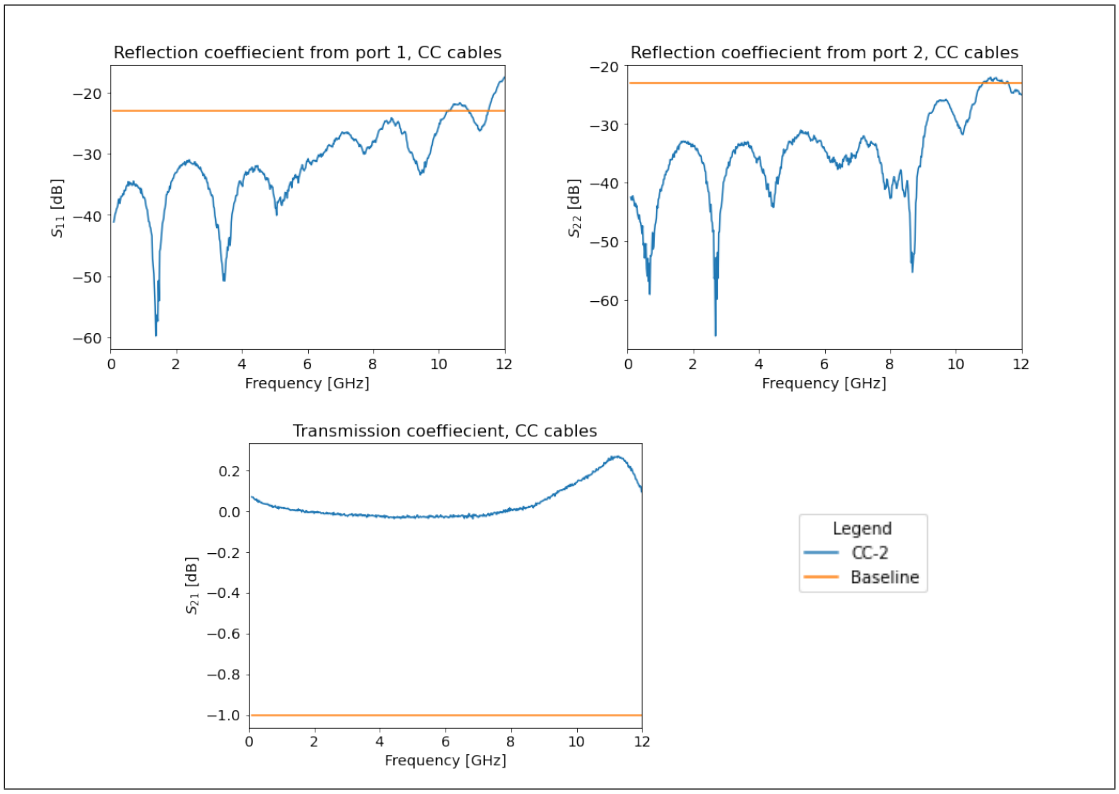

Figure B.7.: Transmission and reflection coefficients of CC-2, the only CC cables we have already prepared. It is important to notice that the baseline for the reflection coefficients is -23 dB.

Critical values of the scattering parameters [dB]			
Cable	Max S11	Max S22	Min S21
SC-1	-16.2	-15.2	-0.8
SC-2	-16.2	-15.6	-0.6
SC-3	-17.3	-20.2	-1.4
SC-4	-17.4	-19.0	-0.6
CC-2	-17.5	-22.0	0

Table B.2.: Critical values for each cable. The measure's unit is dB.

B.4.4. PPS measurements

The reflection and transmission coefficients of the PPS cables have to be analysed in a different way, since the pump signal is characterized by $\nu_{pump} = 17.54$ GHz and it does not make sense to consider the scattering parameters only up to 12 GHz. For this reason the pump cables have been measured up to 20 GHz and a different calibration has been used. The results are shown in Figure B.8 From the figure it is clear that these cables

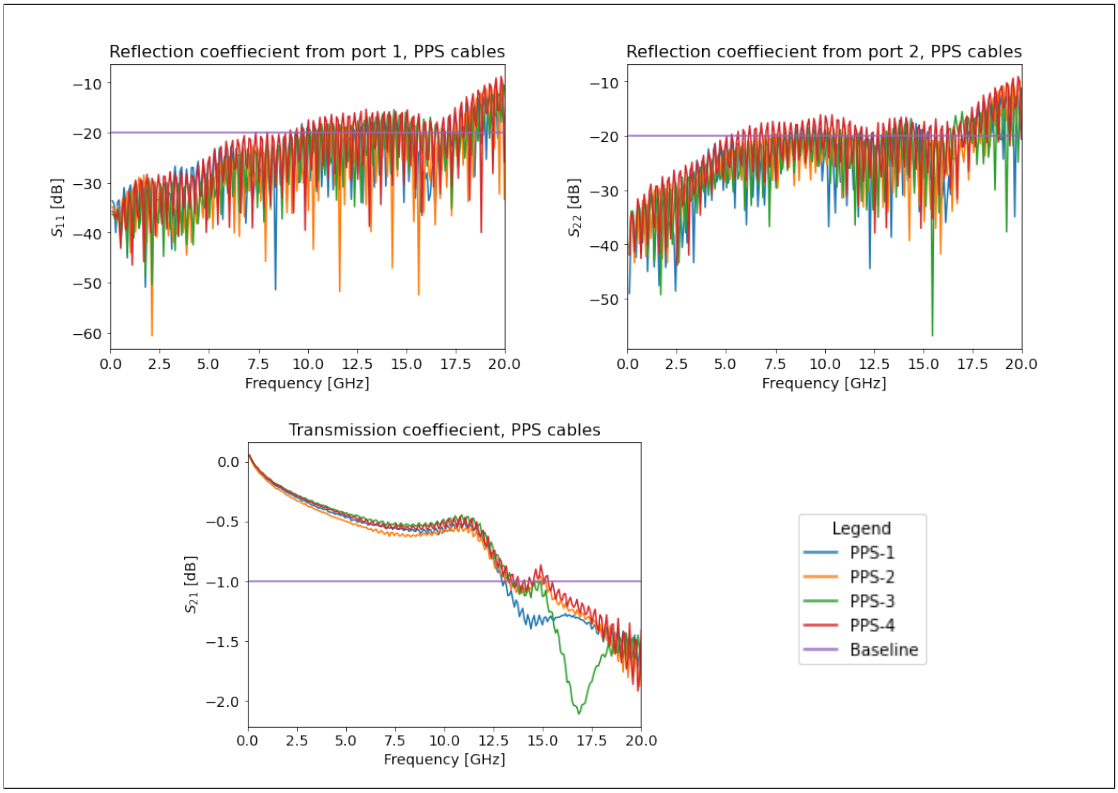

Figure B.8.: Transmission and reflection coefficients of all the PPS cables. The scattering parameters have been measured up to 20 GHz.

follow the specification up to 10 GHz and, after it, they exceed the baseline. However, since the pump signal is a strong signal and can be increased during an experiment, they should not represent a problem and they could probably be not discarded. The only cable that I would discard is PPS-4 since its reflection coefficients are higher compared to the others PPS cables.

Bibliography

1. Feynman, R. P. Simulating Physics with Computers. *International Journal of Theoretical Physics* **21,** 467–488. https://doi.org/10.1007/BF02650179 (1982).
2. Shor, P. W. Polynomial-Time Algorithms for Prime Factorization and Discrete Logarithms on a Quantum Computer. *SIAM Journal on Computing* **26,** 1484–1509. https://doi.org/10.1137/S0097539795293172 (1997).
3. Nation, P. D., Blencowe, M. P., Rimberg, A. J. & Buks, E. Analogue Hawking Radiation in a dc-SQUID Array Transmission Line. *Phys. Rev. Lett.* **103,** 087004. https://link.aps.org/doi/10.1103/PhysRevLett.103.087004 (8 Aug. 2009).
4. Preskill, J. Quantum Computing in the NISQ era and beyond. *Quantum* **2,** 79. ISSN: 2521-327X. https://doi.org/10.22331/q-2018-08-06-79 (Aug. 2018).
5. Kjaergaard, M. *et al.* Superconducting Qubits: Current State of Play. *Annual Review of Condensed Matter Physics* **11,** 369–395. https://doi.org/10.1146/annurev-conmatphys-031119-050605 (2020).
6. Pechenezhskiy, I., Mencia, R. & Nguyen, L. The superconducting quasicharge qubit. *Nature* **585,** 368–371. https://doi.org/10.1038/s41586-020-2687-9 (2020).
7. Chu, Y. & Gröblacher, S. A perspective on hybrid quantum opto- and electromechanical systems. *Applied Physics Letters* **117.** https://doi.org/10.1063/5.0021088 (15 2020).
8. Clerk, A., Lenhnert, P. & et. al. Hybrid quantum systems with circuit quantum electrodynamics. *Nature Physics* **16,** 257–267. https://doi.org/10.1038/s41567-020-0797-9 (2020).
9. Chu, Y. *et al.* Quantum acoustics with superconducting qubits. *Science* **358,** 199–202. https://www.science.org/doi/abs/10.1126/science.aao1511 (2017).
10. Chu, Y. *et al.* Creation and control of multi-phonon Fock states in a bulk acoustic-wave resonator. *Nature* **563,** 666–670. https://doi.org/10.1038/s41586-018-0717-7 (2018).
11. Hann, C. T. *et al.* Hardware-Efficient Quantum Random Access Memory with Hybrid Quantum Acoustic Systems. *Phys. Rev. Lett.* **123,** 250501. https://link.aps.org/doi/10.1103/PhysRevLett.123.250501 (25 Dec. 2019).
12. Triqueneaux, S., Sentis, L., Camus, P., Benoit, A. & Guyot, G. Design and performance of the dilution cooler system for the Planck mission. *Cryogenics* **46,** 288–297. ISSN: 0011-2275. https://www.sciencedirect.com/science/article/pii/S0011227505001700 (2006).
13. Leggett, A. J. Superfluidity. *Rev. Mod. Phys.* **71,** S318–S323. https://link.aps.org/doi/10.1103/RevModPhys.71.S318 (2 Mar. 1999).

14. Zu, H., Dai, W. & de Waele, A. Development of dilution refrigerators—A review. *Cryogenics* **121,** 103390. ISSN: 0011-2275. https://www.sciencedirect.com/science/article/pii/S001122752100148X (2022).

15. Pobell, F. *Matter and Methods at Low Temperatures* https://doi.org/10.1007/978-3-540-46360-3 (Springer Berlin, Heidelberg).

16. BlueFors, C. *Manual BF-LD-SERIES, Cryogen-free Diluition Refrigerator System* ().

17. Uhlig, K. "Dry" dilution refrigerator with pulse-tube precooling. *Cryogenics* **44,** 53–57. ISSN: 0011-2275. https://www.sciencedirect.com/science/article/pii/S0011227503001905 (2004).

18. Krinner, S., Storz, S. & Kurpiers, P. Engineering cryogenic setups for 100-qubit scale superconducting circuit systems. *EPJ Quantum Technology* **6.** https://doi.org/10.1140/epjqt/s40507-019-0072-0 (2019).

19. Eichler, C. *Quantum Science with Superconductin Circuits lecture notes* (2021).

20. Glazman, L. I. & Catelani, G. Bogoliubov Quasiparticles in Superconducting Qubits. *SciPost Phys. Lect. Notes,* 31. https://scipost.org/10.21468/SciPostPhysLectNotes.31 (2021).

21. Serniak, K. *et al.* Hot Nonequilibrium Quasiparticles in Transmon Qubits. *Phys. Rev. Lett.* **121,** 157701. https://link.aps.org/doi/10.1103/PhysRevLett.121.157701 (15 Oct. 2018).

22. Frattini, N. E., Sivak, V. V., Lingenfelter, A., Shankar, S. & Devoret, M. H. Optimizing the Nonlinearity and Dissipation of a SNAIL Parametric Amplifier for Dynamic Range. *Phys. Rev. Applied* **10,** 054020. https://link.aps.org/doi/10.1103/PhysRevApplied.10.054020 (5 Nov. 2018).

23. Kaufmann, N. *Fabrication of a SNAIL Parametric Amplifier, Semester thesis* ().

24. *Autodesk Inventor* https://www.autodesk.com/products/inventor/.